UNIVERSITY OF OSLO

MASTER THESIS

Leaf area impacts on climate feedbacks in the Arctic – A sensitivity study using Norwegian Earth System Model (NorESM)

Author:
Qian SONG

Supervisors:
Frode STORDAL
Hui TANG

Master of Meteorology

August 15, 2017

University of Oslo

Abstract

The Faculty of Mathematics and Natural Sciences
Department of Geosciences

Master of Meteorology

Leaf area impacts on climate feedbacks in the Arctic – A sensitivity study using Norwegian Earth System Model (NorESM)

by Qian SONG

Using the Norwegian Earth System Model (NorESM), we have simulated the climate response to lengthening of the vegetation growing season in the Arctic by modifying the leaf area index (LAI) temporal distribution. We have applied the climate feedback responses analysis method (CFRAM) to decompose the surface temperature changes into partial temperature contributions of individual feedback processes; albedo, water vapor, cloud and aerosols, and non-radiative process of sensible heat flux, latent heat flux, surface dynamics and atmospheric dynamics. The decrease of albedo in the Arctic is associated with the increase of LAI due to lengthening of the vegetation growing season. The changes of albedo lead to a rising of surface temperature in the Arctic. The temperature and albedo changes are larger in the early growing season than in the late season. The sensible heat flux exhibits a relatively strong response to the LAI increase in the Arctic, while the latent heat flux exhibits less changes. The cloud fraction increase in the 50-80°N belt, where the Arctic vegetation was mainly changed. The result of annual mean surface temperature decomposition suggests that in the radiative process, albedo is the primary contribution to surface temperature change, the water vapor exhibits a moderate and positive contribution to the surface temperature change, whereas the changes in clouds show a weak and negative impact on surface temperature, and the aerosols show little contribution. The result of seasonal mean surface temperature decomposition suggest that the climate response due to individual feedback process is more pronounced during spring and summer, when the vegetation starts growing, and the amplitude of partial temperature differences decrease during autumn, towards the end of the vegetation growing season.

Acknowledgements

Firstly, I would like to express my sincere gratitude to my supervisor Professor Frode Stordal for his guidance of my study. He always patiently helped me whenever I ran into trouble or had a question about my thesis.

I would also like to thank my co-supervisor Postdoc Hui Tang for his support. He helped me a lot with the modelling of my study, he gave lots of very valuable comments on my thesis.

Besides my supervisors, I would like to thank my classmates and friends, Susanne, Anais and Sarah. Thanks for your company and helping me through the stressful last several months. I would like to thank all my schoolmates for the fun we had in my two years study live.

Many sincere thanks goes to the teachers of Department of Meteorology and Oceanography for their patience, motivation, immense knowledge and good teaching.

Finally, I must express my very profound gratitude to my mother for providing me with unfailing support and continuous encouragement throughout my years of study. This accomplishment would not have been possible without her. Thank you.

Contents

List of Figures

List of Tables

List of Abbreviations

CFRAM	**C**limate **F**eedback **R**esponse **A**nalysis **M**ethod
LAI	**L**eaf **A**rea **I**ndex
PFTs	**P**lant **F**unctional **T**ypes
NorESM	**N**orwegian **E**arth **S**ystem **M**odel
CCSM	**C**ommunity **C**limate **C**ystem **M**odel
RRTMG	**R**apid **R**adiative **T**ransfer **M**odel **G**lobal version
McICA	**M**onte Carlo **I**ndepent **C**olumn **A**pproximation
NH	**N**orthern **H**emisphere
AMJ	**A**pril **M**ay **J**une
JJA	**J**une **J**uly **A**ugust
ASO	**A**ugust **S**eptember **O**ctober
PAP	**P**attern **A**mplitude **P**rojection coefficient
NDVI	**N**ormalized **D**ifference **V**egetation **I**ndex
ENSO	**E**l **N**ino **S**outhern **O**scillation

Chapter 1

Introduction

Vegetation has been considered as a important aspect of climate system (Pielke et al., 1998). Vegetation affect climate mainly through evapotranspiration and albedo, which primarily impact the radiation surface received and the radiation reflected/emitted from earth to atmosphere (Jeong et al., 2012, Swann et al., 2010). Vegetation also affect atmosphere through biochemical processes, such as photosynthesis and volatile organic compounds emission (Fehsenfeld et al., 1992, Richardson et al., 2013). These processes can affect the greenhouse gases in the atmosphere and change the atmospheric composition. Changes in vegetation distribution of different plant types in different area have the ability to change the weather and the climate in both local and global region (Chapin III et al., 2000).

Recent studies show several important changes of vegetation in response to global warming in the mid-high latitude of North Hemisphere and the Arctic. Myers-Smith et al., 2015 exhibited a large increase in the extent of shrub across Arctic based on sites observation from 1950-2010. Liu et al., 2006 revealed a significant positive vegetation-climate feedback, and vegetation variability is predominantly driven by temperature in middle and high latitude of North Hemisphere. Sykes, 2009 predicted that the vegetation zones move latitudinally towards the North pole. Global warming, especially in the North Hemisphere, is likely to lead to a suitable environment to those species which require warmer and more moist conditions.

The Arctic amplification - surface air temperature change tends to be larger in the Arctic region than in the other region of the globe or the global average, is considered as inherent feature of climate system. Albedo feedback mainly drives the Arctic amplification through changes of sea ice extent and snow cover (Serreze and Barry, 2011).

The Arctic amplification may promotes the vegetation migration and growing season lengthen in Arctic, since the high latitude plants is sensitive to temperature change. We are interested in whether the vegetation changes affect the Arctic amplification. Therefore, in this study, we use climate model to simulate how vegetation growing season lengthen impact on Arctic climate. To better understand the contributions of different climate feedback process to surface temperature changes, the climate feedback response analysis method (CFRAM) is applied (Lu and Cai, 2009, Cai and Lu, 2009).

The CFRAM is a new framework for estimating individual climate feedbacks in climate system, which formulation is based on the energy balances in an atmosphere-surface column. The CFRAM has been used to understand the radiative and non-radiative forcings in temperature changes due to El Nino Southern Oscillation (ENSO) (Deng, Park, and Cai, 2012). It has also been used to quantify the biases of climate models due to individual feedback processes (Park et al., 2014). Hu et al., 2017 used the CFRAM to estimate the different feedback processes between two decadal climate states. Here we use the CFRAM to assess the contributions of individual climate feedback processes to temperature changes associated with lengthening of vegetation growing season in the Arctic.

Chapter 2

Background

2.1 Earth energy budget and feedback process

2.1.1 Earth energy budget

Climate changes on the earth is overall driven by the global energy balance between the absorption of energy flow at earth surface and outgoing energy flow of the planet. The earth energy budget describes a bunch of various types and magnitudes of energy flow at earth system. It includes both radiative components and non-radiative components (such as thermal conduction and convection and energy leaving by evaporation). On spatial and time average, the earth climate system can be regarded as in a equilibrium state, and the amount of incoming radiation is balanced by the amount of outgoing radiation.

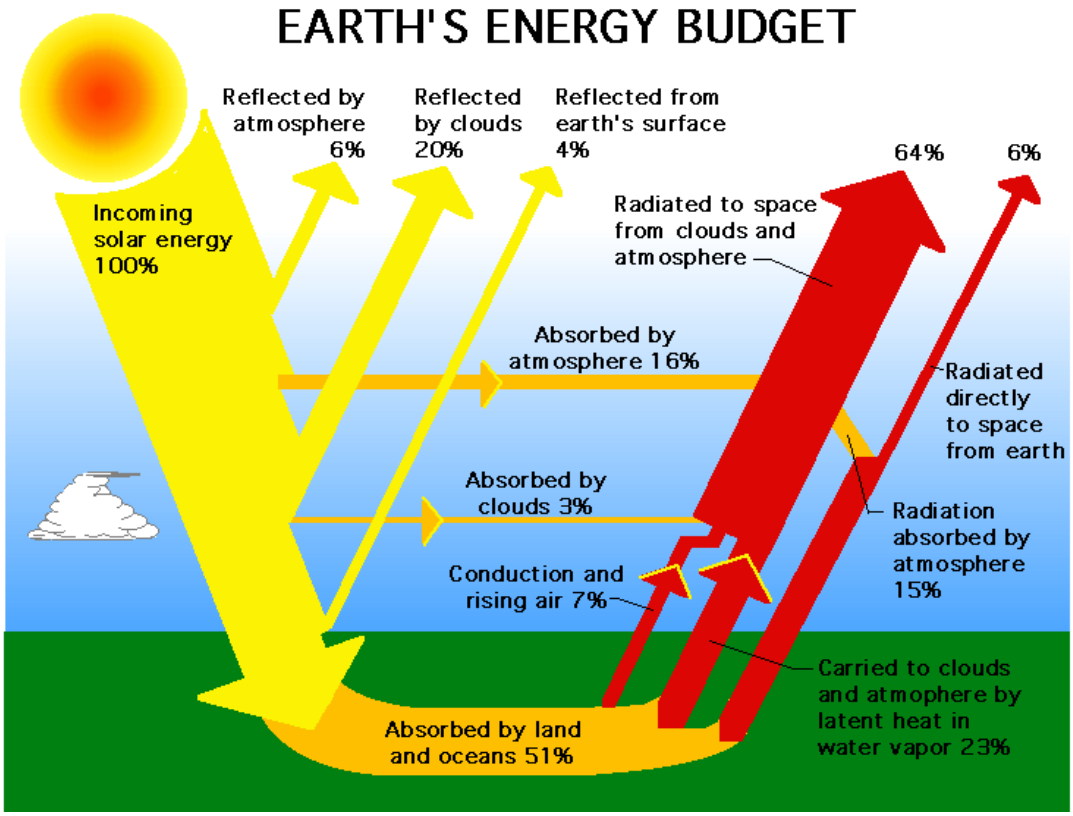

Figure 2.1: Illustration of global energy budget of Earth refer from *Earth's Radiation Budget Facts* 2011.

Fig. 2.1 shows the energy flows of the earth energy budget. The incoming solar insolation is the source of earth's energy, about half of insolation can be absorbed by earth surface, about 20% of insolation is absorbed by atmosphere (water vapor, aerosols, gases and ozone) and cloud, the rest 30% insolation is reflected to the space by atmosphere, cloud and earth surface. Thus totally about 70% solar insolation is absorbed by earth system, which induces the increase of earth temperature. The temperature doesn't infinitely rise, as the earth will emits more radiative flux back to the space with increasing temperature. If the emission is less than absorption, that cause the earth warming and the earth will emit more infrared energy to bring the earth back to balance, and if emission is greater than absorption, the earth will become cooler and reduce the emission to keep the balance (Fig. 2.1).
Stephens et al., 2012 showed a small energy imbalance about 0.6 Wm^{-1} based on observation during decade 2000-2010, which results in a surface warming. This additional heating of our planet primarily entered into the ocean of South Hemisphere (Stephens and L'Ecuyer, 2015). In high latitude, cloud effect is mainly dominated by shortwave reflection whereas in lower latitude the shortwave and longwave cloud effect are largely offset (Stephens and L'Ecuyer, 2015). Trenberth et al., 2015 showed the monthly variability of earth energy budget. At surface, the increased cloud reduces the incoming solar insolation that cools the surface, which in turn reduces outgoing longwave radiative flux, and this phenomenon often reverses in the next month, that corresponds to the earth energy balance adjustment.

2.1.2 Climate feedback mechanism

Albedo

The surface albedo is mainly determined by snow-ice and vegetation. The common feature in snow-ice-albedo feedback is, over ocean, warming leads to the lengthening of the sea-ice melting season which decreases the global mean albedo. This increases the absorption of solar insolation and reduces the shortwave radiation reflection, that further warms the earth surface and melts the sea-ice. Over land, warming leads to earlier spring melt of snow in high latitude, which strengthens the solar energy absorption and leads to the increase of surface longwave radiative flux and sensible heat flux, that further increases the air temperature and enhances the snow melting (Fig. 2.2).
Besides the snow-ice-albedo feedback, the vegetation-albedo feedback attracts more attention recently, since several researches have found that the global warming promotes the poleward migration of vegetation (Seddon et al., 2016, Sykes, 2009, Jeong et al., 2012, Loranty, Goetz, and Beck, 2011, Miller and Smith, 2012). The expansion of vegetation to high latitude decreases the surface albedo in the region and also causes the rising of solar insolation absorption and reduces the shortwave radiation reflection, and increases the air temperature. the increase of vegetation also strengthens the latent and sensible heat flux to atmosphere (Fig. 2.3).

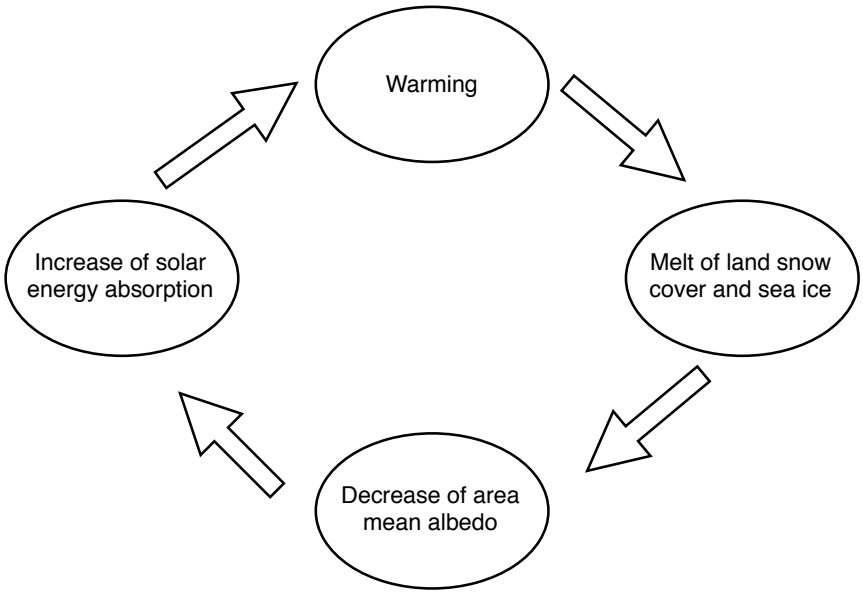

Figure 2.2: Illustration of ice-albedo feedback

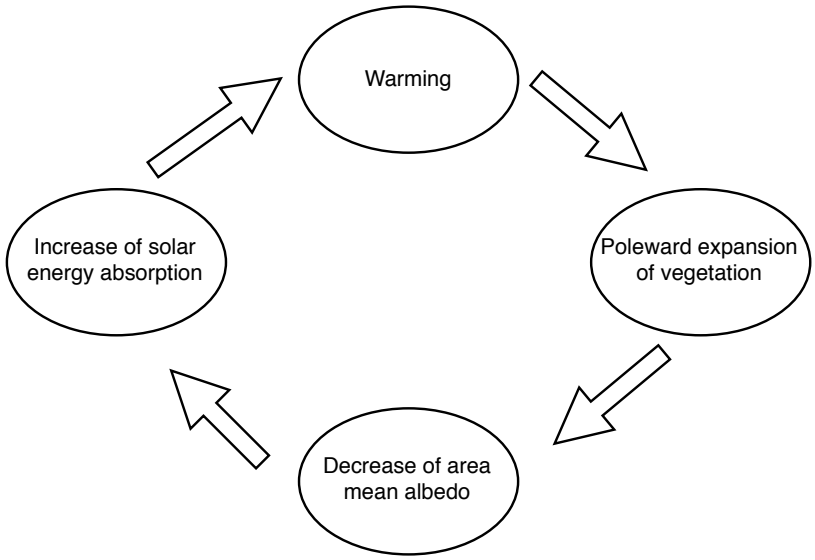

Figure 2.3: Illustration of vegetation-albedo feedback

Cloud

Different from albedo-climate feedback, cloud has more complex impact on climate energy budget. Warming leads to stronger evaporation which supplies more water vapor for cloud formation. The increase of cloud fraction cloud lead to warming effect by trapping the surface emission below the cloud base, and the increased cloud fraction also could lead to cooling effect by increasing the reflection of incoming shortwave. The cloud warming effect is regarded as the longwave cloud forcing, and the cooling effect is regarded as the shortwave cloud forcing. The longwave cloud forcing is a function of cloud temperature, height and emissivity, and the shortwave cloud forcing is a function of cloud transmittance, surface albedo, and the solar zenith angle (Shupe and Intrieri, 2004).

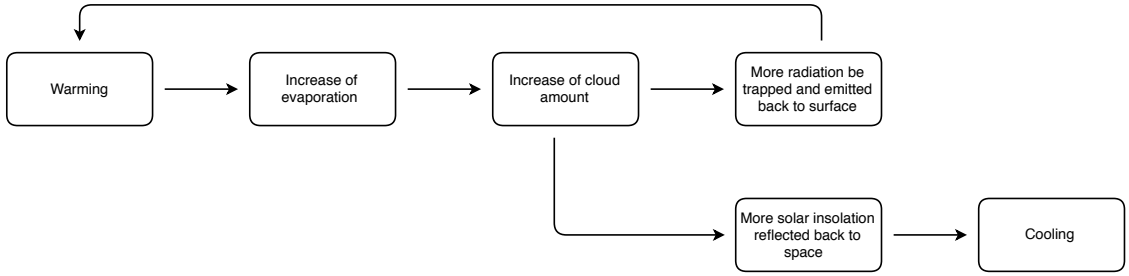

Figure 2.4: Illustration of cloud feedback

Water Vapor

Climate response to atmospheric water vapor changes is simply illustrate in Fig. 2.5. Water vapor is known as one of the greenhouse gases, which traps the longwave radiation in lower troposphere and increases surface air temperature. Warming environment promotes evaporation and increases the loading of atmospheric moisture, consequently more absorbed longwave radiation is emitted back to the surface by water vapor.
Besides warming-induced water vapor increasing, increase of vegetation mass (LAI increasing) promotes the evapotranspiration and releases more water vapor to atmosphere. Beringer et al., 2005 worked with site observation data in the Arctic. It is found that the transition from shrub to forest with increasing LAI, increases the evapotranspiration and leads to positive precipitation. This results in a positive feedback to further warming Arctic.

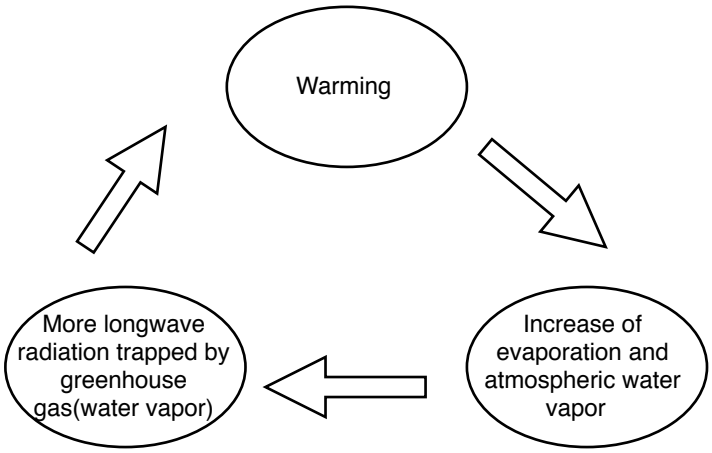

Figure 2.5: Illustration of water vapor feedback

2.2 The climate change status and impacts on vegetation

2.2.1 Climate change status and Arctic amplification

Last several decades, the surface temperature increases rapidly, especially in North Hemisphere. The globally mean surface temperature increased 0.78 °C from period 2003-2012 to 1850-1900. Impacted by the warming, more surface water evaporates, and a high confidence positive precipitation change was found in mid-latitude area of North Hemisphere since 1901. The glaciers of Greenland, Antarctic have lost mass and contributed to sea level rise throughout the 20th century. The snow melting over northern hemisphere in spring is earlier, and the Arctic sea ice extent decreased since 1979 in range of 3.5% to 4.1% per decade. The permafrost temperatures have increased in most regions of Northern Hemisphere, which further increased surface temperature and decreased the snow cover (Pachauri et al., 2014).

The increasing of surface air temperature tends to be larger in Arctic region than other area of North Hemisphere or globe area, that is known as Arctic amplification. The loss of sea ice extent impact the heat flux between atmosphere and surface, the cloud cover, the evaporation and moisture flow in atmosphere. The Arctic amplification is larger in autumn and winter season, moderate in spring and weaker in summer (Serreze and Barry, 2011). The albedo feedback is considered as the primary cause of Arctic amplification, warming induced by greenhouse effect will melt the snow and ice cover of Arctic, the exposed darker surface strengthens the absorption of solar energy, that leads to further warming and further retreat of snow and ice cover. Furthermore, the warming induces the increase of atmosphere water vapor content and cloud amount, that affect the downwelling longwave radiative flux, which further leads to warming surface, especially in winter (Chen et al., 2011). The retreat of the Arctic sea ice cover changes the vertical heat fluxes between Arctic Ocean and the overlying atmosphere, The ice formation in autumn and winter is delayed, that promotes enhanced upward heat fluxes and strengthens the warming at the surface and in the lower troposphere (Serreze et al., 2009).

2.2.2 The vegetation response to climate change in Arctic

A bulk of paper in recent researches which based on observation addressed the issue of shrub expansion to Arctic tundra system (Fraser et al., 2011, Beck and Goetz, 2011, Lin et al., 2012, Tremblay, Lévesque, and Boudreau, 2012). The warming climate supports more suitable environment in high-latitude for vegetation which prefer warmer place, that increase the biomass and extend the growing season (Epstein, Myers-Smith, and Walker, 2013). For the boreal forest, several studies mentioned the tree growth was positively related to summer temperature till about 1950, but there were less positive signals after 1950, the explanation of this is the increasing drought stress of soil moisture, which limited the growth (Andreu-Hayles et al., 2011, Ohse, Jansen, and Wilmking, 2012).
Pearson et al., 2013 use the model with scenario of 2050s to simulate the vegetation response to climate change, the results show that half of vegetation will shift to a different physiognomic species and woody cover will increase 52%, and the vegetation distribution shifts will result in an overall positive feedback to climate that leads to further warming in Arctic region. Kaplan and New, 2006 simulated Arctic climate changes and vegetation responses to four greenhouse gas emissions scenarios with anthropogenic rising the temperature for 2°C above preindustrial levels. Results in these four scenario show a significant increase of potential forest area, in the warmest scenario, there is a large increase of temperate forest area presented. Jeong et al., 2012 simulated the response of vegetation to double present CO_2, they found a notable northward expansion and greening of plants over the high-latitudes, north of 60N. The fractional covers of all PFTs greatly increase over high-latitude, particularly for the Arctic grass group which more than doubled its fractional coverage. Miller and Smith, 2012 simulated the tundra vegetation response to Arctic warming, the regions dominated by forest show the significant increase of LAI, whereas the regions dominated by shrub have more modest and variable changes, that the increases of LAI occur near the tree-line, and decreases in LAI also occur near the deciduous shrub dominated area.

2.2.3 Feedback of vegetation change to climate

Loranty, Goetz, and Beck, 2011 studied the different types and heights of Arctic tundra vegetation, and suggested that even a small increase in shrub height occurring over shorter time scales or changes in difference vegetation type may have energy impact in local region, associated with albedo effect. Loranty et al., 2014's results also suggested that differences in boreal biomes and spatial variation of PFTs strongly influence the high latitude albedo dynamics. Through model simulation, Bonfils et al., 2012 found the large-scale shrub expansion triggered substantial regional atmospheric warming in spring and summer through direct albedo changes, and this effect may impact the strength of the indirect sea-ice albedo effect. Jeong et al., 2011 showed that greening in high latitude induces strong albedo decrease, while moderate albedo decrease is present in mid-latitude. They suggest that the impact of albedo feedback may vary with the latitude. Miller and Smith, 2012 simulated the climatic impact of tundra vegetation changes in the Arctic, and the result shows the decrease of albedo in winter is larger than summer. And it also shows that there is a spatial variability in winter albedo change, regions dominated by forest and shrub show more remarkable reduction in albedo than the other regions.

The net cloud forcing effect may vary with different latitude and season. Vavrus et al., 2009 simulated the cloud response to greenhouse forcing in Arctic, and shows the clouds become cloudier, especially in autumn and over sea ice area. The simulation shows a positive correlation between cloud amount and surface air temperature changes, except

summer. Chen et al., 2011 simulated climate with a moderately increasing greenhouse gas scenario from 1850 to 2100, and shows the sensitivity of downwelling longwave flux to cloud changes is largest in winter and weakest in summer.Laguë and Swann, 2016 projected the climate response to mid-latitude afforestation, and reveal that in water limited region, increasing forest cover may dries out the troposphere and leads to clouds amount decreasing. Hence, the warming-induced cloud fraction increasing also required the moisture hold ability of local atmosphere. They also found that the increasing of high-latitude cloud induces a negative net radiation and consequential cooling effect. Besides the direct effect, changes of cloud also influence other climate feedback. For example, thin cloud let more radiation pass through than thick cloud, that strength the positive albedo feedback (Kay et al., 2016).

Swann et al., 2010 simulated how the climate response to adding deciduous trees on bare ground in the Arctic. And they suggested, with LAI increased, the greenhouse warming by additional water vapor may trigger a positive feedback and amplify the ongoing warming. The change of precipitation minus evaporation is positive in the Arctic, but negative in the lower latitude, suggesting that there is a net import of water vapor from lower latitudes to high latitude. Jeong et al., 2012 studied the greening in high latitude and show that the additional increased moisture-holding capability due to the warmer temperature and the enhanced surface evapotranspiration by enhanced vegetation activity may induce an increase in tropospheric moisture content over the high-latitude and Arctic region, this feedback associated with water vapor increases may be amplified in the growing season by the vegetation feedback.

Chapter 3

Data and Method

3.1 Model description and data

The Norwegian Earth System Model (NorESM1) is a comprehensive coupled model based on Community Climate System Model (CCSM), with an advanced chemistry-aerosol-cloud-radiation interaction schemes in atmospheric module (CAM-Oslo), and an isopycnic coordinate ocean model which developed based on Miami Isopycnic Coordinate Ocean Model (MICOM) included ocean carbon cycle biogeochemical ocean module (Bentsen et al., 2013). The atmospheric module of NorESM, namely, CAM-Oslo, is a version of CAM, with modified schemes for aerosol-radiation and aerosol-clouds interaction that are developed in Oslo. CAM-Oslo involves the effect of biogenic primary organics aerosol and methane sulfonic acid from oceans, calculates mass concentration of aerosols in 4 size mode: nucleation, Aitken, accumulation, coarse. CAM-Oslo has the comprehensive simulation of aerosol life cycles, and also includes the effect of aerosol populations on cloud albedo and cloud lifetime (Kirkevåg et al., 2013).
In this study we use NorESM with CAM5-Oslo module, data ocean model, prescribed sea ice and pre-industry initial condition. The atmosphere model, CAM5-Oslo, is a version of CAM5 with modified chemistry-aerosol-cloud-radiation interaction schemes. Use an rapid radiative transfer model (RRTMG) as the radiation scheme. The model resolution is 1.9x2.5 in horizontal and 30 vertical layers in atmosphere. We have performed two model experiments, one is pre-industry control run using default vegetation cover and LAI parameters (CTRL), the other using the same boundary conditions expect the modified LAI parameters which are manually changed in temporal distribution to simulate the lengthening of vegetation growing season (LAIRUN) (see section 3.2). Each experiment run for 50 years and the last 10 years results are used to get required input variables for CFRAM analysis.

Climate feedback response analysis method (CFRAM) calculation requires radiative energy differences of each feedback processes which can't directly obtain from NorESM output, therefore the extra radiative transfer experiments are necessary to represent the radiative flux and retrieve energy differences of feedback processes. In this study, we use an offline radiative transfer model (RRTMG) from Atmospheric & Environmental Research (AER) for CFRAM analysis. RRTMG is an rapid radiative transfer model which use the correlated-k approach to calculate radiation fluxes and heating rates. RRTMG is extensively used in many global and regional models. RRTMG is divided into longwave model with 16 spectral bands and 14 band in shortwave. Molecular absorbers of longwave model are water vapor, carbon dioxide, ozone, nitrous oxide, methane, oxygen, nitrogen, and the common halocarbons. Modeled sources of extinction in shortwave model include water vapor, carbon dioxide, ozone, methane, oxygen, aerosols, and Rayleigh scattering, the discrete-ordinate-method radiative transfer algorithm DISORT is used in shortwave model to perform the radiative transfer calculations for multiple

scattering (Clough et al., 2005).
The input variables of pressure, temperature, humidity, albedo, solar insolation and clouds-related properties are requisite for RRTMG calculations. In this study, we use annual mean and seasonal mean values from the last 10 years NorESM experiments for longwave radiative transfer experiments, and multi-year hourly mean values of temperature, pressure, solar insolation, and albedo related variables are applied for shortwave radiative transfer experiments.

3.2 Modification of leaf area index (LAI)

With a strong polar warming amplification effect over Arctic, recently several study based on observation report that vegetation from lower latitude start to invade and expand to higher latitude.

The Leaf Area Index (LAI) is defined as leaf area per unit land area. It is an important quantity of plant canopies which influence the surface radiation reflectance and aslo is an candidate of hydrological cycle. Prescribed LAI data is got from the input surface data of land model. To focus on Arctic region and simulate the characteristics of plants increasing in amount and expanding of vegetation growth season, I modified LAI in the area north than 50°N with seven selected species those grow in Arctic and have seasonal growth cycle. The species of vegetation is defined by Plant Functional Types (PFTs) in land model, the PFTs types and the corresponding species shown in table. 3.1, the selected species are marked. To modify LAI, I assume a threshold $thld_{i,j}$ that defined as the difference between summer and winter mean LAI divide by five, and calculate the differences $\Delta LAI^m_{i,j}$ of two adjacent months,

$$\Delta LAI^m_{i,j} = LAI^m_{i,j} - LAI^{m+1}_{i,j} \tag{3.1}$$

$$thld_{i,j} = \frac{\overline{LAI^{6,7,8}_{i,j}} - \overline{LAI^{12,1,2}_{i,j}}}{5} \tag{3.2}$$

then, circularly compare the differences with threshold. Here m is the number of one perticular month, i and j specify the latitude and longitude. The onset month is the first month when $\Delta LAI^m_{i,j}$ is greater than $thld_{i,j}$. Similarly, the ending month is the month after when $\Delta LAI^m_{i,j}$ less than $thld_{i,j}$(Fig. 3.1).

LAI distribution along time axis is high in summer, low in winter. The growth period is expanded by modifying the LAI temporal distribution, in specifically, by moving the part between onset month and maximum month (the month with maximum LAI value) one month forward and the part between offset month and maximum month one month backward. Onset in January, ending in December or ending before August are not changed. Additionally, the grids with onset in February are manually set to March, and moving the second part till November while ending happened in November (Fig. 3.2).

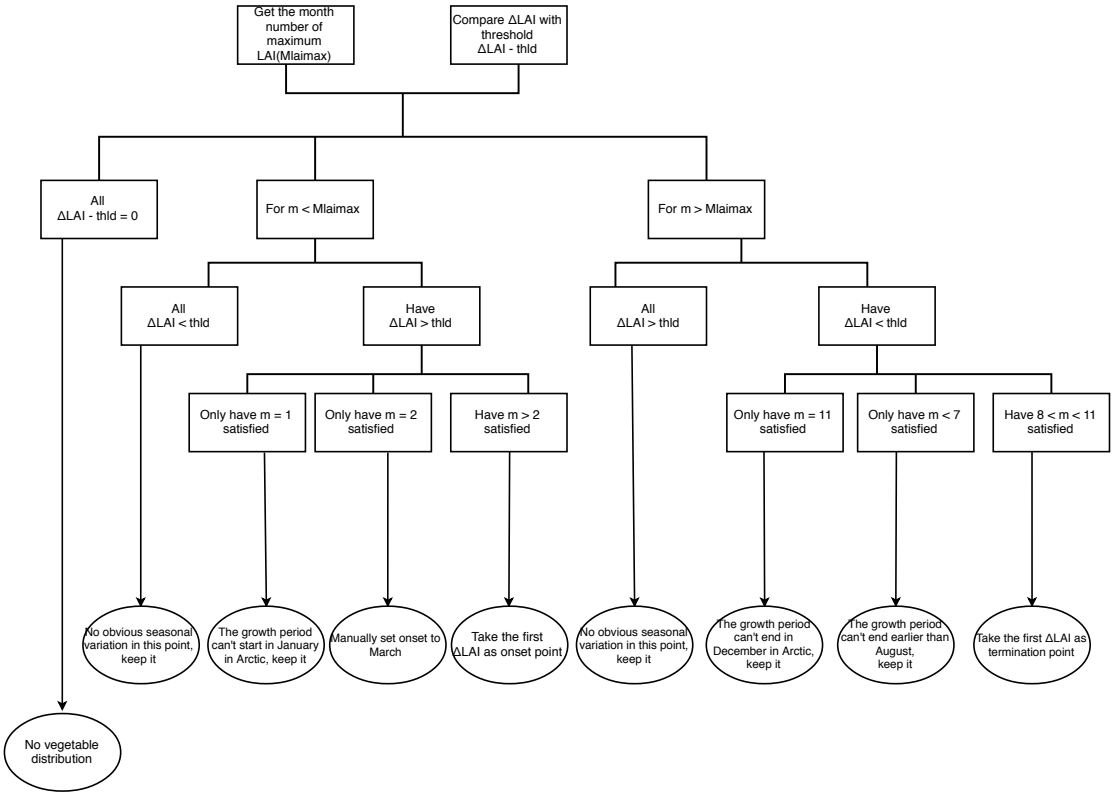

Figure 3.1: Illustration of Leaf area index modification process. m is the number of month, M_{laimax} is the month number of maximum LAI, ΔLAI is the LAI difference of adjacent months, $thld$ is the threshold I defined and calculated in the eq. 3.2

Table 3.1: PFTs types

number of PFTs type in model code	name of selected species
1	needleleaf evergreen temperate tree
2	needleleaf evergreen boreal tree
3	needleleaf deciduous boreal tree
7	broadleaf deciduous temperate tree
8	broadleaf deciduous boreal tree
10	broadleaf deciduous temperate shrub
11	broadleaf deciduous boreal shrub
12	C3 arctic grass
13	C3 non-arctic grass

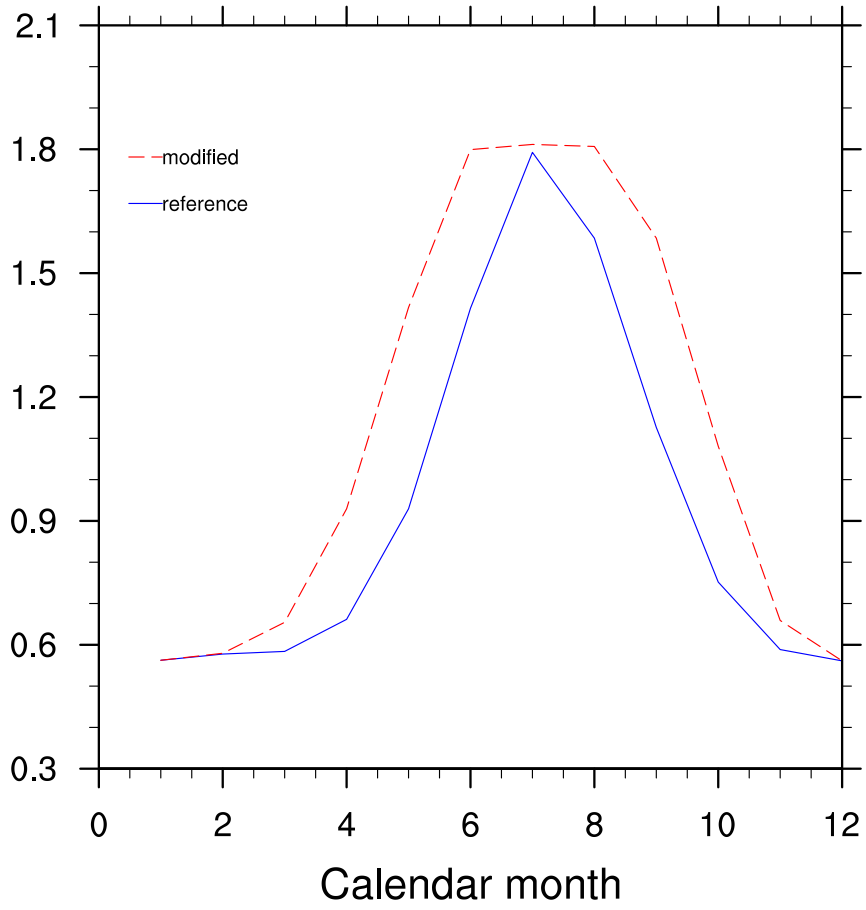

Figure 3.2: Comparison between modification and reference total LAI integrated over all selected PFTs types

3.3 Description of climate feedback response analysis method (CFRAM)

Climate Feedback Response Analysis Method (CFRAM) technique is applied in this work to decompose the temperature contributions of individual feedback process. Following Lu and Cai, 2009 and Cai and Lu, 2009, CFRAM is developed by considering the difference of energy balances in an atmosphere-surface column between two time mean climate states is negligible while these two climate state reach to statically steady.

$$\Delta\frac{\partial E}{\partial t} = \Delta Q^{rad} + \Delta Q^{non-rad} \tag{3.3}$$

Where, $\Delta\frac{\partial E}{\partial t}$ is the difference in energy balance between two time mean climate states, ΔQ^{rad} is the non-temperature induced radiative energy flux and $\Delta Q^{non-rad}$ is the non-radiative energy flux perturbations.
In definition,

$$\Delta Q^{rad} = \Delta S - \Delta R \tag{3.4}$$

Furthermore, the energy differences of individual radiative process and non-radiative process can mathematically represent as:

$$\Delta S = \Delta S^{alb} + \Delta S^{cld} + \Delta S^{aer} + \Delta S^{wv} \tag{3.5}$$

$$\Delta R = \Delta R^{cld} + \Delta R^{aer} + \Delta R^{wv} - \frac{\partial R}{\partial T}\Delta T \tag{3.6}$$

$$\Delta Q^{rad} = \Delta Q^{alb} + \Delta Q^{cld} + \Delta Q^{wv} + \Delta Q^{aer} - -\frac{\partial R}{\partial T}\Delta T \tag{3.7}$$

$$\Delta Q^{rad} = \Delta(S-R)^{cld} + \Delta(S-R)^{wv} + \Delta(S-R)^{aer} + \Delta S^{alb} - \frac{\partial R}{\partial T}\Delta T \tag{3.8}$$

$$\Delta Q^{non-rad} = \Delta Q^{SH} + \Delta Q^{LH} + \Delta Q^{atm-dyn} + \Delta Q^{sfc-dyn} \tag{3.9}$$

Where ΔS is the difference in shortwave radiative flux, ΔR is the difference in longwave radiative flux, ΔQ^{alb},ΔQ^{cld},ΔQ^{wv} and ΔQ^{aer} represent the radiative flux perturbation induced by albedo, cloud, water vapor and aerosol feedback. $\frac{\partial R}{\partial T}\Delta T$ is the longwave radiative flux difference induced by temperature change. ΔQ^{SH},ΔQ^{LH},$\Delta Q^{atm-dyn}$ and $\Delta Q^{sfc-dyn}$ represent the energy difference induced by sensible heat, latent heat, atmospheric dynamics and surface dynamics. Atmospheric dynamics is the energy changes due to convection and large-scale advective energy transport in atmosphere. Surface dynamics is the energy changes of surface turbulent energy exchanges with atmosphere and the horizontal ocean energy transport in surface. Dynamical radiative flux perturbation can not directly retrieve quantity output, but they are available to be calculated base on equation 3.3. Through equation 3.3,3.4 and 3.8, the temperature difference can be obtained as:

$$\begin{aligned}\Delta T =& (\frac{\partial R}{\partial T})^{-1}\{\Delta(S-R)^{cld} + \Delta(S-R)^{wv} + \Delta(S-R)^{aer} + \Delta S^{alb} + \Delta Q^{SH} \\ &+ \Delta Q^{LH} + \Delta Q^{atm-dyn} + \Delta Q^{sfc-dyn}\}\end{aligned} \tag{3.10}$$

In CFRAM, $\frac{\partial R}{\partial T}$ is planck matrix, which represent the radiative flux changes due to temperature variation, and the inversed planck matrix $\frac{\partial R}{\partial T}^{-1}$ products the temperature changes in an particular layer due to radiative flux perturbations of all model layers. In this work, planck matrix derived by cyclically adding 1K temperature to one level and calculating longwave radiative flux difference.

To qualify the contributions of individual process, following Park et al., 2014, a pattern-amplitude-projection (PAP) coefficient is calculated as:

$$PAP_x = A^{-1} \int a^2 \Delta T cos\phi d\lambda d\phi \cdot \frac{A^{-1} \int_A a^2 \Delta T_x \Delta T cos\phi d\lambda d\phi}{A^{-1} \int_A a^2 (\Delta T)^2 cos\phi d\lambda d\phi} \tag{3.11}$$

Where A is the area of considered region, a is average earth radius, ϕ is latitude and λ is longitude. ΔT_x is partial temperature difference of associated individual process. ΔT is total temperature difference. PAP provide a balanced measurement of pattern and amplitude to individual process.

Chapter 4

Result and Discussion

4.1 Setup and evaluation of CFRAM

4.1.1 The use of hourly data

To represent the radiative energy budget with RRTMG, several tests were done before the formal experiments. It is found in the NorESM the albedo is count as 1 while the zenith angle >90 °, that causes the annual/monthly mean albedo output greater than it's actual value, as well as the zenith angle has apparent daily variation which inevitably impacts on the calculations of solar insolation and shortwave transmittance in RRTMG, we consider to conduct 3 tests with daily and hourly input data:

Test 1: all required input data are hourly, calculate the daily mean radiative flux by running RRTMG for 24 times and calculating the average value of 24 hours.
Test 2: similar as test 1, but only hourly inputs of temperature, pressure, zenith angle, albedo, humidity are used.
Test 3: all required input datas are daily, and run RRTMG for 1 time.

The downwelling shortwave radiative flux at surface of test 3 is lower than NorESM output along mid-low latitude. The result from test 1 and test 2 in high latitude are relatively lower than NorESM output, because the solar constant is defined lower than NorESM set in these test runs (Fig. 4.1). The patterns and amplitudes of them are similar to NorESM output. An explanation for the bias in mid-low latitude of test 3 is the absence of daily variation of zenith angle which is essential for calculating shortwave transmittance in the radiative model.

The upwelling shortwave radiative flux at top of model shown in Fig. 4.2 illustrate an apparently high bias in test 3 compared with NorESM output, test 1 and 2. The reason for this high bias is the daily mean albedo input data from NorESM is greater than the natural value, because in NorESM albedo is defined as 1 while there is no incoming solar radiation (Fig. 4.3). In addition, this albedo problem may induced notable error as albedo is one key point of the LAI sensitive experiments of this work. Song, Zhang, and Cai, 2014 aslo apply hourly data in the offline radiative flux calculation of CFRAM, and show the improvement of radiative flux calculation accuracy.

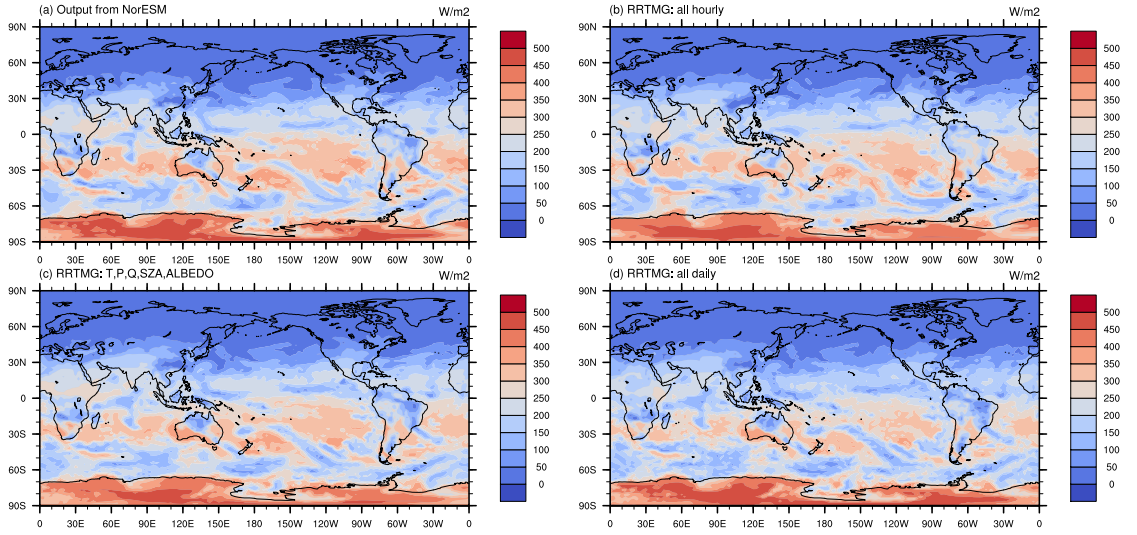

Figure 4.1: The daily downwelling shortwave radiative flux at surface, date of input data is Jan. 5th of first year of last 10 years. **a** output from NorESM, **b** test 1: derived from RRTMG with all input datas are hourly, **c** test 2: similar with test 1 but only input of temperature, pressure, humidity, zenith angle and albedo are hourly, **d** test 3: all input datas are daily.

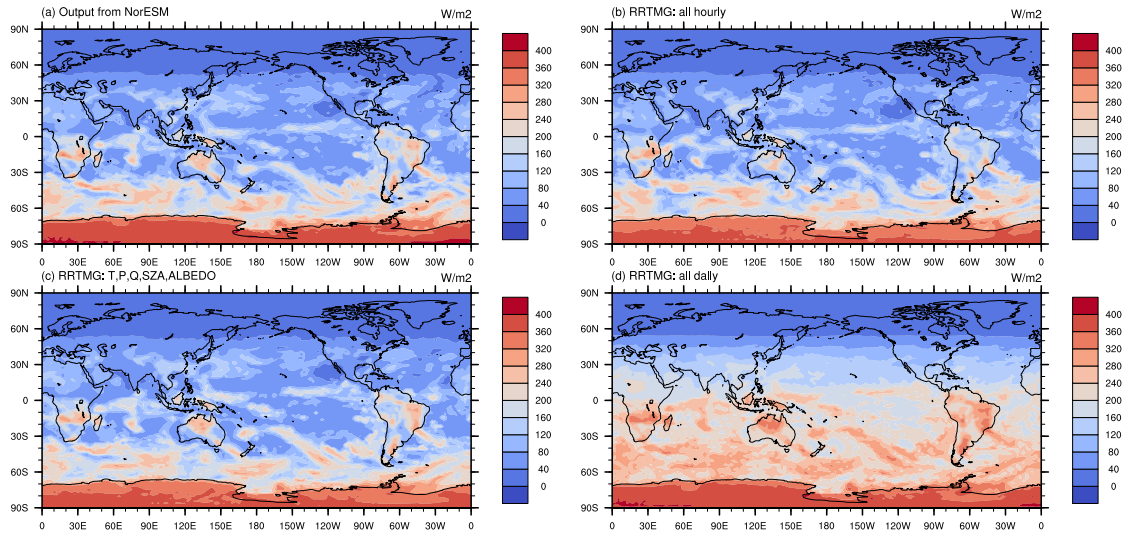

Figure 4.2: The daily upwelling shortwave radiative flux at top of model , date of input data is Jan. 5th of first year of last 10 years. **a** output from NorESM, **b** test 1: derived from RRTMG with all input datas are hourly, **c** test 2: similar with test 1 but only input of temperature, pressure, humidity, zenith angle and albedo are hourly, **d** test 3: all input datas are daily.

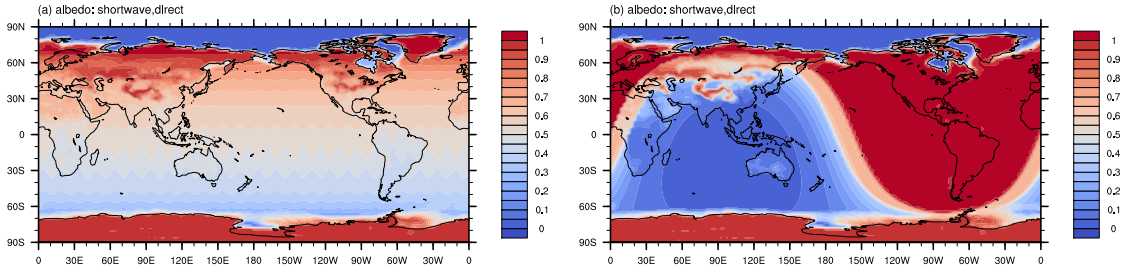

Figure 4.3: Shortwave albedo, direct, date of input data is Jan. 5th of first year of last 10 years. **a** daily mean albedo, **b** albedo of 6 a.m. of Jan. 5th.

We also tests if these three input data set in longwave radiative model produce reliable radiative net flux for CFRAM.

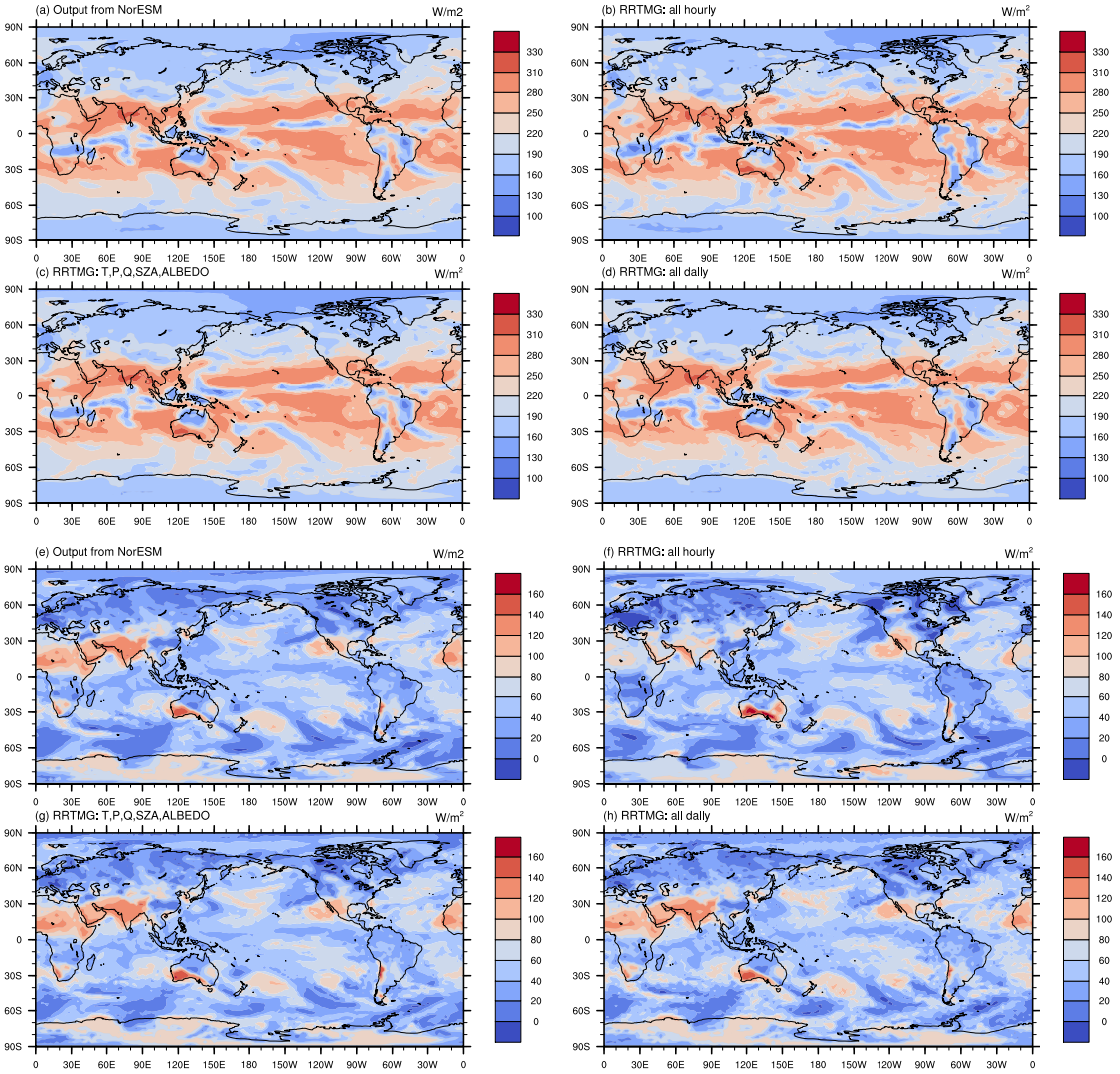

Figure 4.4: The daily net longwave radiative flux at top of model for figure **a b c d** and at surface for figure **e f g h**. Date of input data is Jan. 5th of first year of last 10 years. **a&e** output from NorESM, **b&f** test 1: derived from RRTMG with all input datas are hourly, **c&f** test 2: similar with test 1 but only input of temperature, pressure, humidity, zenith angle and albedo are hourly, **d&h** test 3: all input datas are daily.

Even test with daily input, the test 3 shows little difference with NorESM in net longwave radiative flux, as well as test 1 and test 2 which were conducted with hourly data. This indicates that using longwave model without hourly data is sufficient to simulate longwave radiative flux for CFRAM analysis (Fig. 4.4).

Combining the requirement of reducing the errors derived by the daily varied variables, zenith angle and albedo, and the computation and data storage cost, we use hourly input variables of temperature, zenith angle, albedo, pressure, and humidity for shortwave radiative flux simulation, and use annual/monthly mean data for longwave radiative flux simulation.

4.1.2 Cloud randomization in radiative transfer model

The radiative transfer model I used which includes the Monte Carlo Independent Column Approximation (McICA), an method used in radiative calculation to reduced the errors induced by unresolved cloud fluctuations(Barker et al., 2008). McICA stochastically generates sub-columns of a specific model column, performs radiative transfer calculation on them for individual spectral band, then takes the spectral integration of mean radiative flux over all sub-columns.

$$F = \sum_{k=1}^{k} f(s,k) \tag{4.1}$$

Here is the basic radiative flux calculation equation of McICA and calculate radiative flux profile in one column 4.1 (Hansen et al., 1983), F is the radiative flux integrated in one column, k is spectral intervals and s is sub-column number. However, the radiative transfer calculation of long time mean shown noise in the decomposition result of cloud feedback (Fig. 4.5(a)), which is produced by randomly generation of cloud overlap and McICA sub-columns (Zhang, Jing, and Li, 2014). To evaluate how this noise impact on climate simulation and reduce these by-product, Räisänen, Barker, and Cole, 2005 proposed an improved equation,

$$F = (1-C) f_{clr}(s_{clr},k) + C \sum_{k=1}^{k} [\frac{1}{N_k} \sum_{n=1}^{N_k} f_{cld}(s_{cld,n,k},k)] \tag{4.2}$$

Where C is cloud fraction, f_{clr} and f_{cld} are the radiative flux computed in clear sky and cloudy, N_k is the number of samples for particular spectral band, $s_{cld,n,k}$ represents the nth cloudy sub-column used for the kth spectral interval.

To understand and test this process, experiments of three different sample size are represented. The significant improvement apparent from the comparison of $N_k = 1$ and $N_k = 200$ experiments, with $N_k = 200$, the model recall the radiative flux calculation for 200 times, that effectively increase the signal-noise ratio, furthermore, the improvement between $N_k = 400$ and $N_k = 200$ experiments is limited (Fig. 4.5). This suggests that N_k increasing can efficiently reduce the noise, but it has a limitation, and should be mentioned that N_k increasing requires more CPU hour.

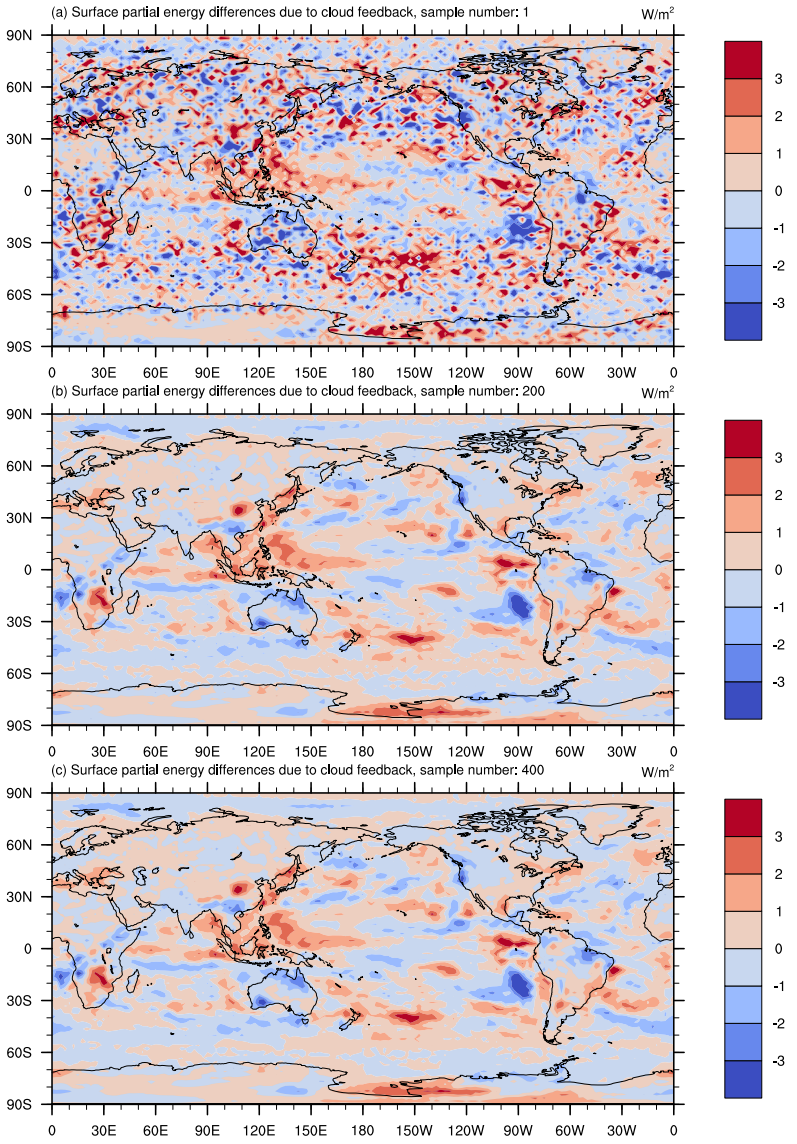

Figure 4.5: Annual mean surface partial energy difference due to cloud feedback. **a** $N_k = 1$, **b** $N_k = 200$, **c** $N_k = 400$.

4.1.3 Choice between cloud optical depth and cloud water path

Additionally, the RRTMG provides two options of cloud input variables: directly specify the optical depths of cloud and calculate cloud optical depths by using cloud water path. In this work, cloud water path is computed by using cloud liquid mixing ratio and cloud ice mixing ratio.

$$CWP_{liq} = r_{liq} \int_{p_m}^{p_{m+1}} dp/g \tag{4.3}$$

$$CWP_{ice} = r_{ice} \int_{p_m}^{p_{m+1}} dp/g \tag{4.4}$$

$$\tag{4.5}$$

Where r_{liq} and r_{ice} is cloud liquid mixing ratio and cloud ice mixing ratio, $\int_{p_m}^{p_{m+1}} dp$ represent the pressure increment between two pressure interface. and g is the gravitational acceleration.

Fig. 4.6 shows that less noise in mid-low latitude when using cloud water path than using cloud optical depth. Hence, I use cloud water path instead of cloud optical depths for radiative transfer calculation in this work.

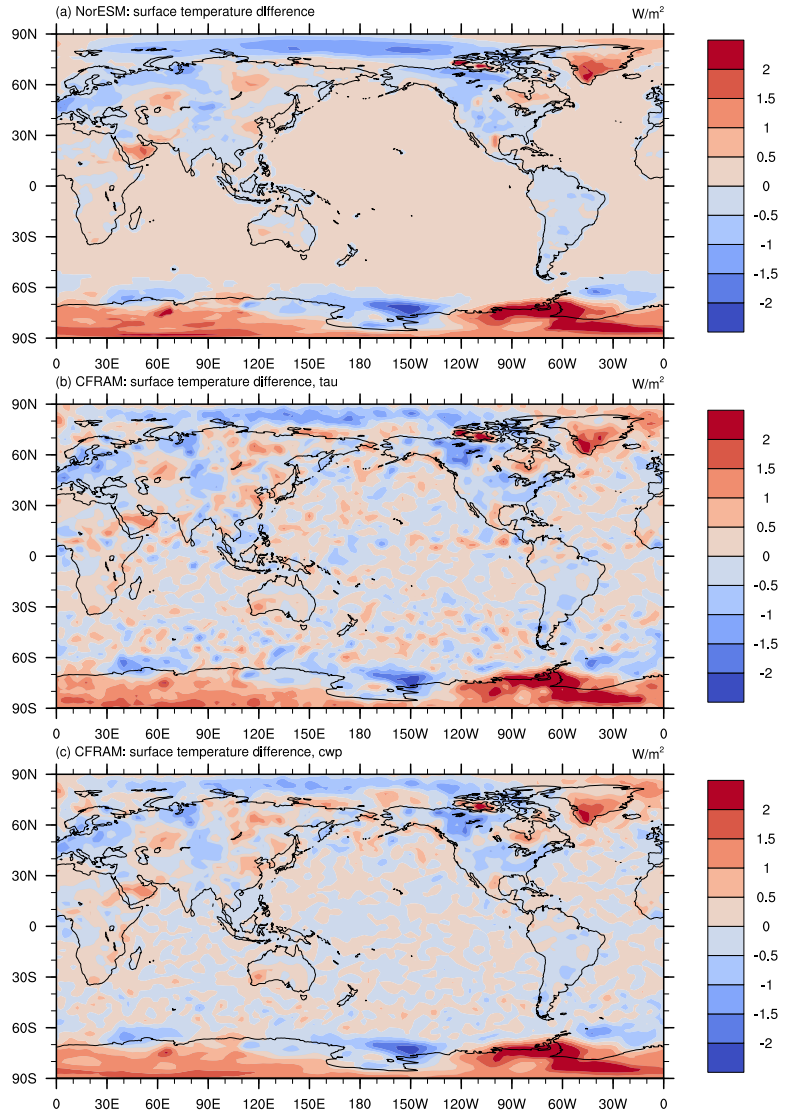

Figure 4.6: Monthly mean surface temperature difference in July. **a** NorESM output, **b** input: cloud optical depth, **c** input: cloud water path.

4.1.4 The derivations of surface dynamics and atmosphere dynamics of CFRAM

The difference of energy storage in two time mean climate states are considered to be negligible according to the theory of CFRAM. This can be used to derive dynamical contributions from the equation. In detail, there are three ways to derive dynamical contributions,
The method A is using radiation difference calculated from RRTMG.

$$\Delta Q^{dyn} = -[\Delta Q^{rad}_{rrtmg} + \Delta Q^{SH} + \Delta Q^{LH}] \tag{4.6}$$

The method B is getting radiation difference by summing up all the partial radiation differences due to individual radiative feedback process and thermal effect.

$$\Delta Q^{dyn} = -[\Delta Q^{alb} + \Delta Q^{cld} + \Delta Q^{aer} + \Delta Q^{wv} - \frac{\partial R}{\partial T}\Delta T^{tot}_{noresm} + \Delta Q^{SH} + \Delta Q^{LH}] \tag{4.7}$$

The method C is using radiation difference calculated from NorESM, the model output.

$$\Delta Q^{dyn} = -[\Delta Q^{rad}_{noresm} + \Delta Q^{SH} + \Delta Q^{LH}] \tag{4.8}$$

The partial temperature of dynamical contributions are calculated as:

$$\Delta T^{dyn} = \left(\frac{\partial R}{\partial T}\right)^{-1} \Delta Q^{dyn} \tag{4.9}$$

Where ΔQ^{rad}_{rrtmg} is the energy difference derived from RRTMG, ΔQ^{rad}_{noresm} is the energy difference computed from NorESM output, $\frac{\partial R}{\partial T}\Delta T^{tot}_{noresm}$ is the radiation changes due to the temperature change. the temperature difference from NorESM output is used in thermal effect term of method B.
In the Fig. 4.7, the surface temperature difference derived by using method A shown the similar pattern and amplitude with NorESM output (Fig.4.7(b)), and method C derived surface temperature difference by using radiation difference from NorESM shown several anomalies in NH low-latitude and east Asia (Fig.4.7(d)), because the radiative calculation between the offline-model and NorESM is not the same, there are some difference exist, for example NorESM includes more species of aerosol which participate to radiative process. Even through method B, which calculate the total radiation difference through summing up all the partial energy difference, shown the most similar plot (Fig.4.7(c)), it still can not be used.
Back to the equations, for method B (Eq. 4.7), all the partial temperature difference are cancelled and only the temperature difference left when calculate the total temperature difference, that cause the result of total temperature difference derived from CFRAM is nearly same as NorESM output. This generates an circular argument, which make the decomposition meaningless (Eq. 4.11-4.15).

Hence, in this study, I will present all decomposition results of CFRAM with using of hourly zenith angle, albedo, temperature, pressure and humidity for shortwave model and time mean data for longwave model, cloud water path for cloud optical depths calculation, 200 samples for cloud randomization and the total energy difference calculated from RRTMG to derive dynamics contribution.

$$\Delta Q^{dyn} = -[\Delta Q^{alb} + \Delta Q^{cld} + \Delta Q^{aer} + \Delta Q^{wv} - \frac{\partial R}{\partial T}\Delta T^{tot} + \Delta Q^{SH} + \Delta Q^{LH}] \tag{4.10}$$

$$\Delta T^{dyn} = \left(\frac{\partial R}{\partial T}\right)^{-1} \Delta Q^{dyn} \tag{4.11}$$

$$\Delta T^{dyn} = -\left(\frac{\partial R}{\partial T}\right)^{-1} (\Delta Q^{alb} + \Delta Q^{cld} + \Delta Q^{aer} + \Delta Q^{wv} - \frac{\partial R}{\partial T}\Delta T^{tot}_{noresm} + \Delta Q^{SH} + \Delta Q^{LH}) \tag{4.12}$$

$$\Delta T^{dyn} = -(\Delta T^{alb} + \Delta T^{cld} + \Delta T^{aer} + \Delta T^{wv} + \Delta T^{SH} + \Delta T^{LH} - \Delta T^{tot}_{noresm}) \tag{4.13}$$

While total temperature difference is calculated as,

$$\Delta T^{tot}_{cfram} = \Delta T^{alb} + \Delta T^{cld} + \Delta T^{aer} + \Delta T^{wv} + \Delta T^{dyn} + \Delta T^{SH} + \Delta T^{LH} \tag{4.14}$$

$$\Delta T^{tot}_{cfram} = \Delta T^{tot}_{noresm} \tag{4.15}$$

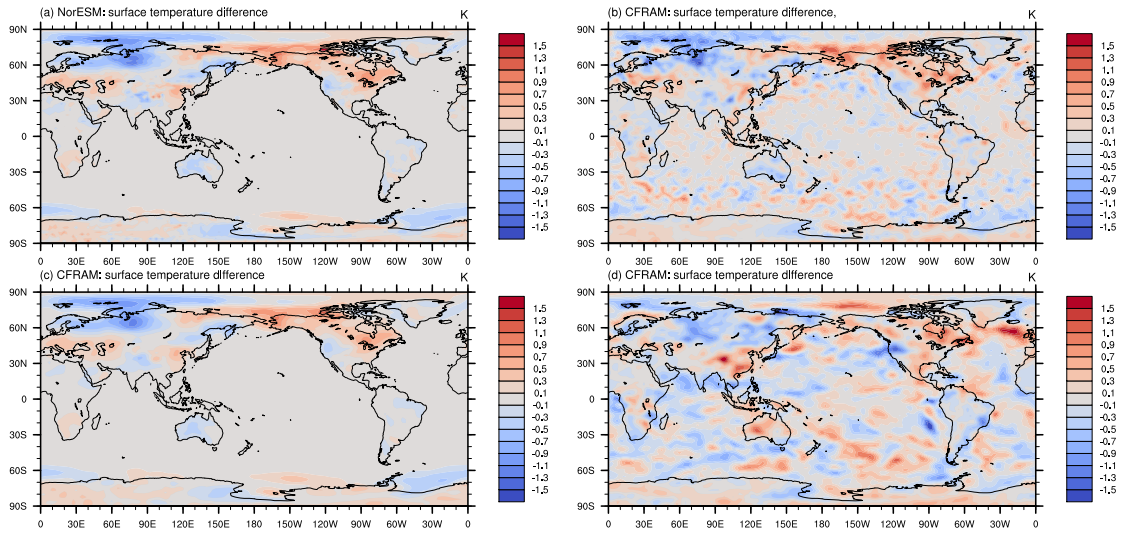

Figure 4.7: The annual mean surface temperature difference. **a** output from NorESM, **b** derived from CFRAM, calculate dynamics contribution by using radiation differences from RRTMG results (Eq. 4.6), **c** derived from CFRAM, calculate dynamics contribution by using the sum of partial energy differences and thermal effect (Eq. 4.7), **d** derived from CFRAM, calculate dynamics contribution by using radiation differences from NorESM output (Eq. 4.8).

4.2 The climate impact of lengthening the growing season

In this section, the responses of NorESM to leaf area modification in Arctic are presented.

Surface temperature largely changes over NH, significantly warming effect shown in mid-high North America and a part of East Asia, but cooling effect over high latitude Eurasia (Fig. 4.8) and moderate cooling in mid-latitude. The temperature changes shows sensitive responses to the albedo changes (Fig. 4.9) in high latitude area of NH after growing season is lengthened, but albedo is not the only contribution to temperature change. The surface temperature also shown the sensitivity to the trend of albedo changes in LAI modification area (50°N-90°N). The vegetation growing season lengthening caused by LAI increase in spring-summer and summer-autumn period lead to albedo decrease in these two periods, surface temperature changes also correspond to this result. Specially, the result shows that the surface temperature and albedo are more sensitive to LAI changes in the spring-summer period than the autumn period (Fig. 4.10, 4.11), even through the increment of LAI in these two period is similar (Fig. 3.2). This may cause by the different solar insolation of these two period. Surface temperature also shown decreasing over NH high latitude in winter while albedo has a related less difference.

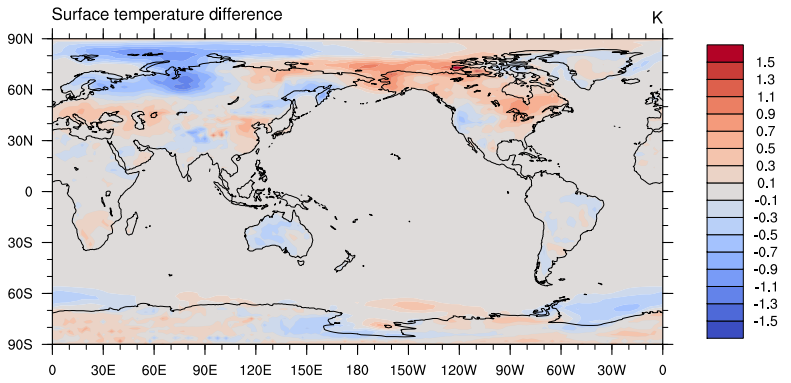

Figure 4.8: Annual mean surface temperature difference between the leaf area modified experiment and control run.

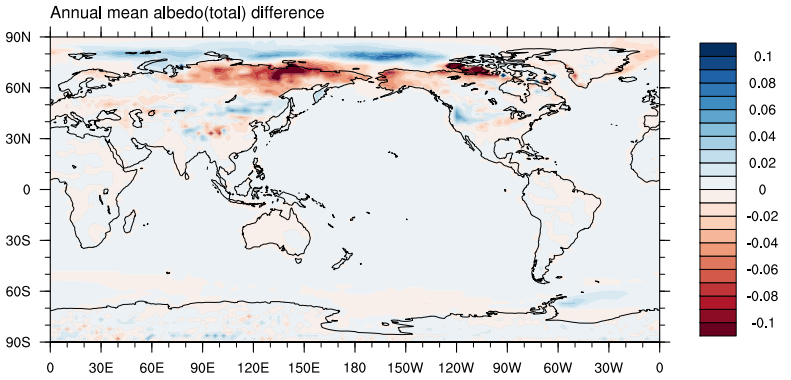

Figure 4.9: Annual mean albedo(total) difference between the LAIRUN and CTRL, the albedo is separated into longwave albedo and shortwave albedo in the model output

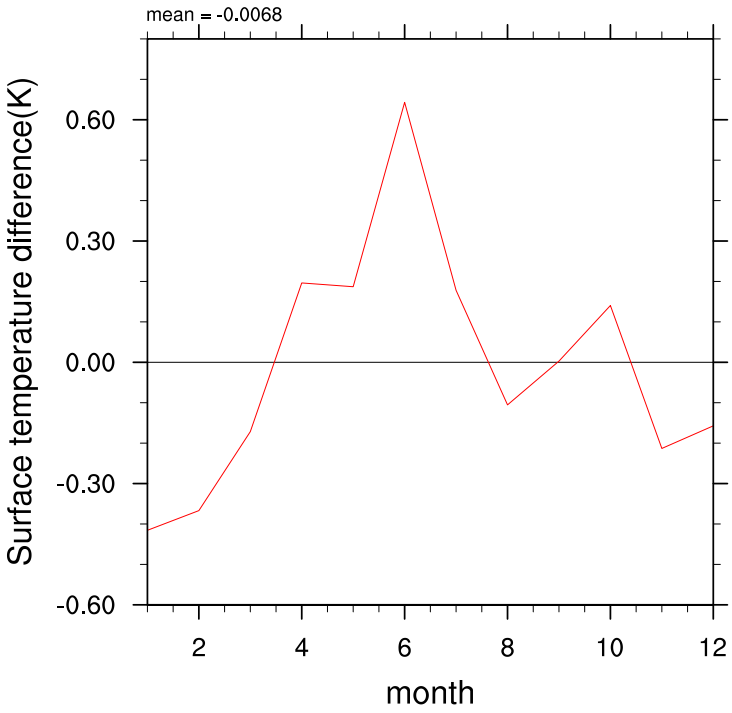

Figure 4.10: Monthly trend of surface temperature difference between the LAIRUN and CTRL, integrated in the area of LAI modfication (50°N - 90°N).

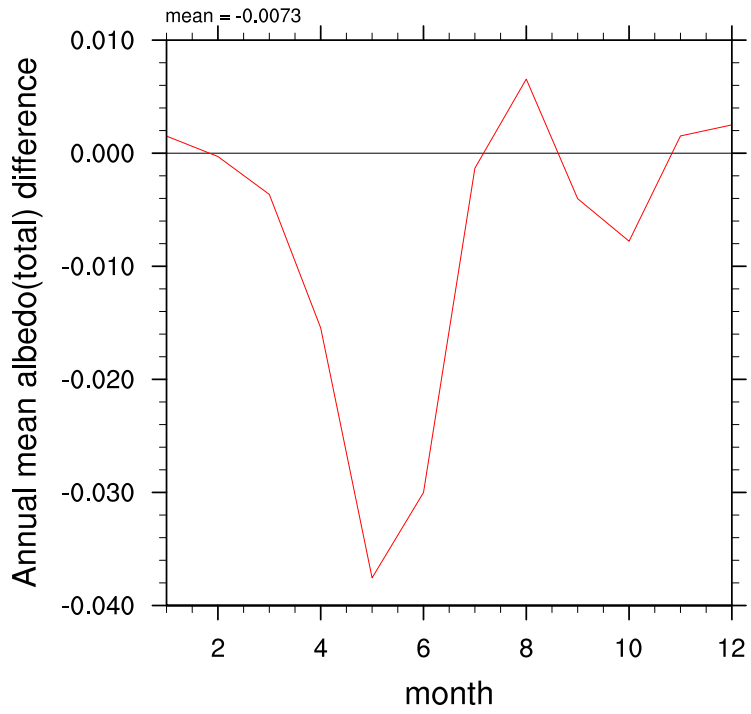

Figure 4.11: Monthly trend of albedo (total) difference between the LAIRUN and CTRL, integrated in the area of LAI modfication (50°N - 90°N).

Shortwave net radiative flux shown significant increasing in middle and high latitude over continent, which result is consistent with albedo decreasing. Similar, the longwave net radiative flux small increases in middle and high latitude. As a result of these surface radiation changes, the surface received net energy in Arctic (Fig. 4.12). Sensible heating obviously increasing in high-latitude of North America and East Asia, that show the response of temperature increased in these areas, in contrast, latent heating difference mainly dominated in ocean, but both sensible heating and latent heating shows positive differences in the north ocean of Scandinavia (Fig. 4.13).

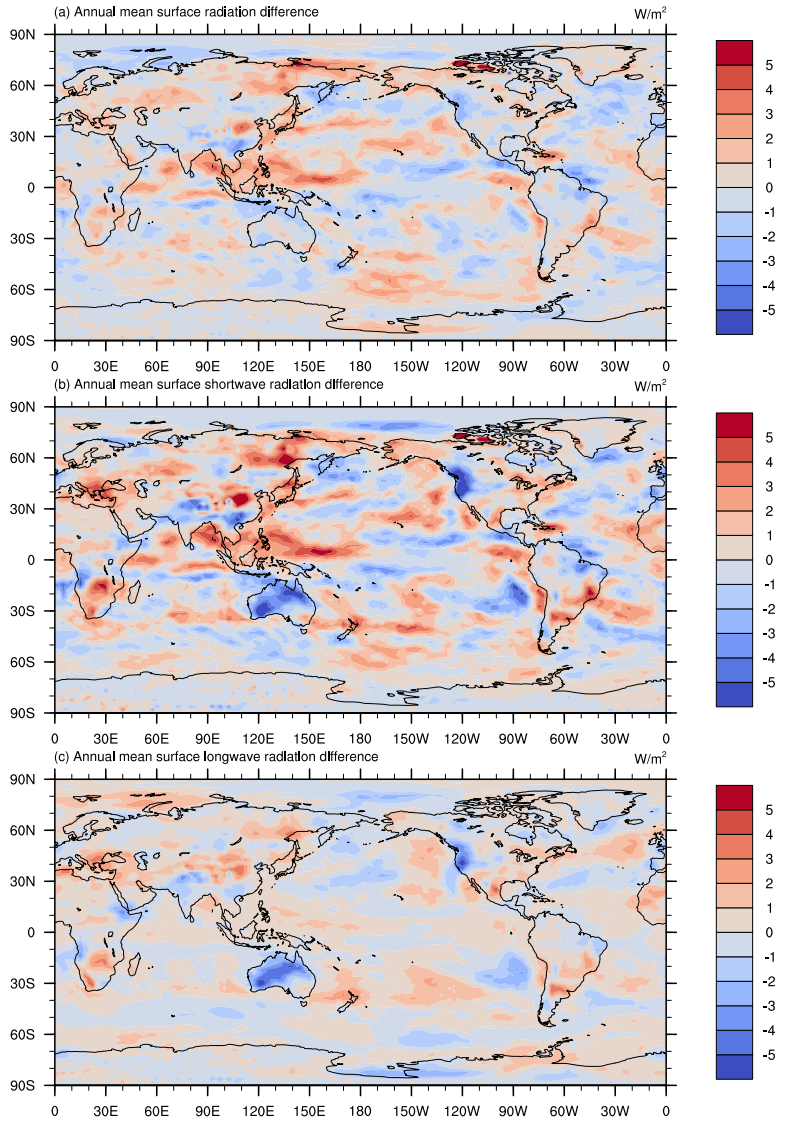

Figure 4.12: **a** Annual mean surface energy difference, **b** Annual mean surface shortwave radiation difference, **c** Annual mean surface longwave radiation difference.

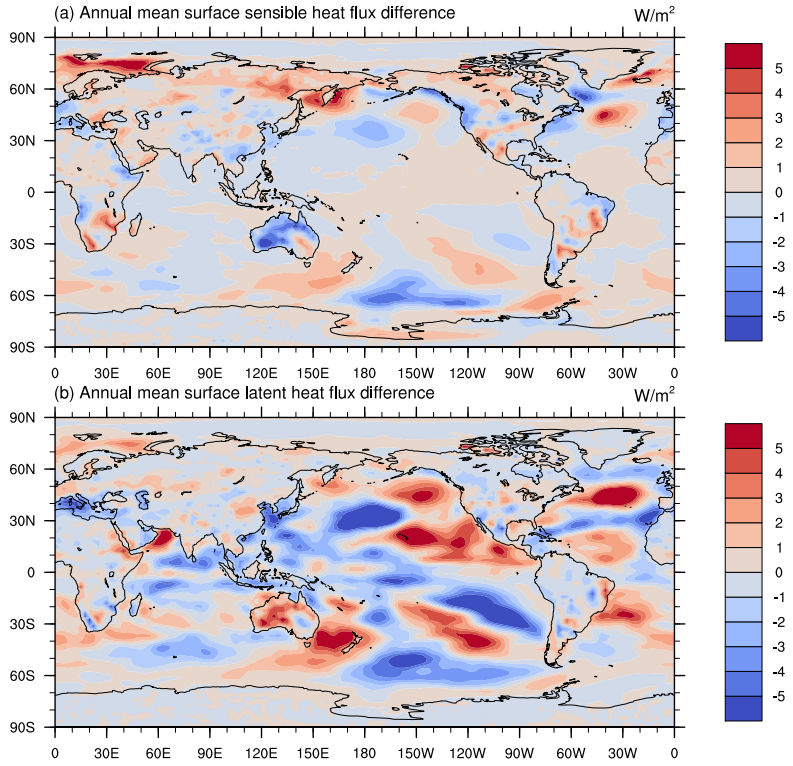

Figure 4.13: **a** Annual mean surface sensible heat flux difference, **b** Annual mean surface latent heat flux difference.

Humidity of low troposphere increases in north-west America, north-east Asia and NH mid-high latitude, it decreases in NH mid-low latitude, north Eurasia and Arctic ocean (Fig. 4.14), which is in consistency with the lack of low cloud in Arctic ocean (Fig. 4.15). With growing season lengthening, decreased albedo induces more incoming shortwave, that enhances warming effect. For the area, where has less humidity, temperature decreasing is observed. Fig. 4.15 also shows that, compare with low cloud, more middle and high cloud appear in NH high-latitude, Fig. 4.16 also show the similar result, less cloud over 80°N-90°N, while cloud fraction increases in 60°N-80°N, middle and high cloud increase in 30°N-60°N, and mid-low latitude has a moderate cloud loss, these are in agreement withVavrus et al., 2009 findings which showed under warming effect, Arctic high cloud has relatively large increases. And the low clouds significantly increase in north-side of 50°N where the LAI modification applied suggesting that the vegetation growing season lengthening can affect regional region cloud changes.

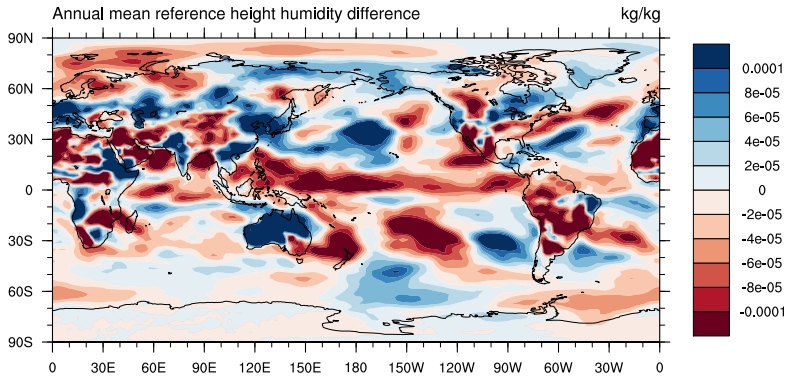

Figure 4.14: Annual mean reference height humidity difference.

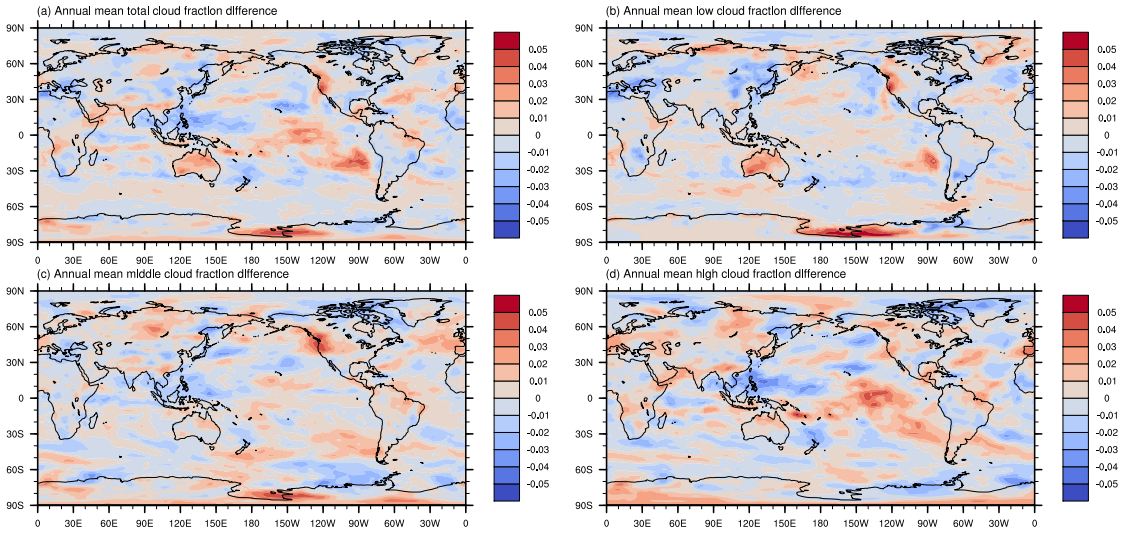

Figure 4.15: Annual mean cloud fraction difference. **a** total cloud, **b** low cloud, **c** middle cloud, **d** high cloud.

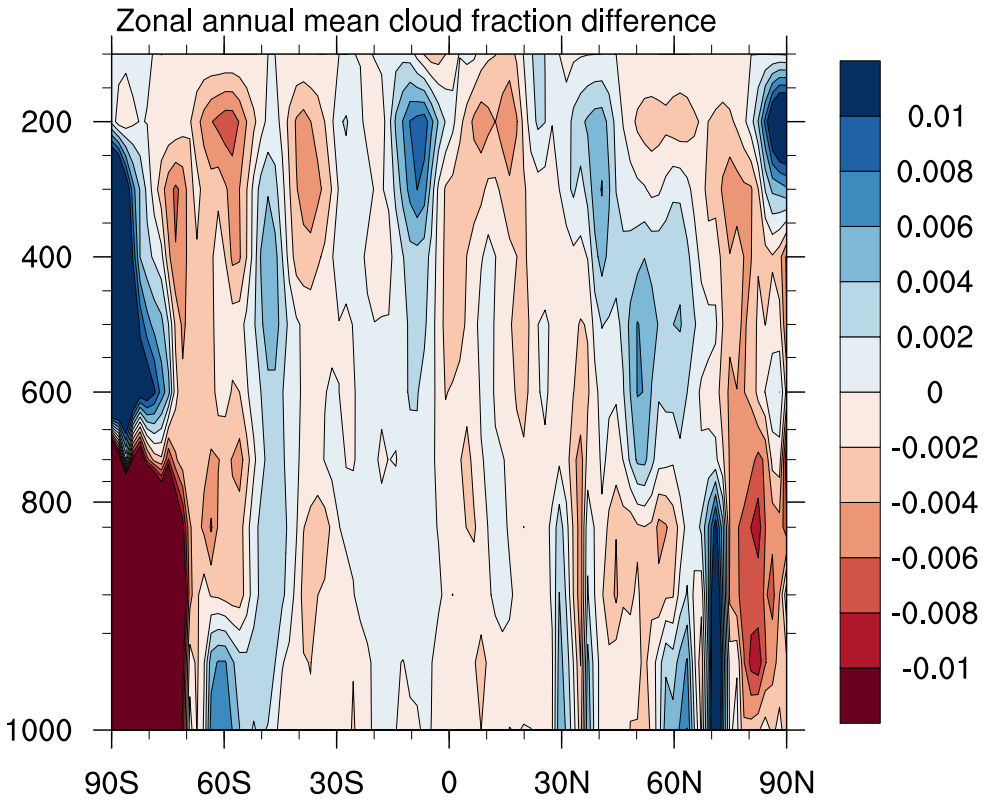

Figure 4.16: Annual mean cloud fraction difference.

4.3 Surface temperature contributions of individual climate feedback

4.3.1 Annual response

Fig. 4.17(a) is annual mean surface temperature difference from NorESM output, and total surface temperature difference derived from CFRAM is shown in Fig.417(b), which is the sum of partial surface temperature differences due to different climate feedbacks. ΔT_{cfram} shows similar pattern and amplitude by comparing with ΔT_{noresm}. Fig. 4.17(c)-(j) shows the decompositions of annual mean surface temperature due to individual feedback process and non-radiative process from CFRAM. The albedo contributes significantly to north-east Asia and north west America, where albedo decreases (Fig. 4.9). Cloud induces warming effect in Eurasia and North America, but weaker than albedo warming effect, and cloud cooling effect shows in high latitude and north Arctic ocean, where cloud decrease(Fig. 4.16), cloud warming effect is also observed in NH low-latitude, tropics and mid-high latitude of south hemisphere. Water vapor shows a small contribution to surface temperature difference, it has warming effect in 40°N - 70°N of NH, except north-east coast of North America. And water vapor contribution also shows cooling effect in the northern ocean of Scandinavia and north-west of Russia land, that slightly contribute to cooling in these area. aerosol has little contribution to surface temperature difference. Sensible heat has a little cooling in north-east Asia where temperature increases due to albedo effect. Sensible heat has little effect over ocean, in contrast latent heat strongly impacts ocean surface temperature differences. Surface dynamics impact land surface temperature by horizontal heat diffusion in the soil and transport of energy by river run-offs, and it contributes to warming over land. The contribution of atmospheric dynamics to surface temperature represents the temperature changes due to atmospheric dynamic process in upper layers, and it shows a significant cooling in high-mid latitude of NH.
To quantify the contribution of individual process to the temperature changes due to LAI modification, I calculate the pattern-amplitude-projection (PAP) coefficient following Hu et al., 2017. Fig. 4.18 shows PAP coefficients for all radiative and non-radiative process. The annually regional mean surface temperature difference is mainly affected by surface dynamics, atmospheric dynamics, albedo and water vapor. However, the cloud feedback lead to a weak cooling of surface temperature. The impacts of aerosols, latent heat and sensible heat are relatively small. Fig. 4.19 represent PAP coefficient over land in the same region, which shows similar results, and it also shows that atmospheric dynamics has relatively limited impact on surface temperature over land. Surface dynamics is the major contribution of annual surface temperature change, albedo also shows remarkable impact on surface temperature. Changes in high-latitude albedo lead to a increase in absorption of incoming solar radiation. With plant growing season lengthened, clouds fraction increase, that reduces the solar energy reach to surface, producing a negative contribution to surface temperature.

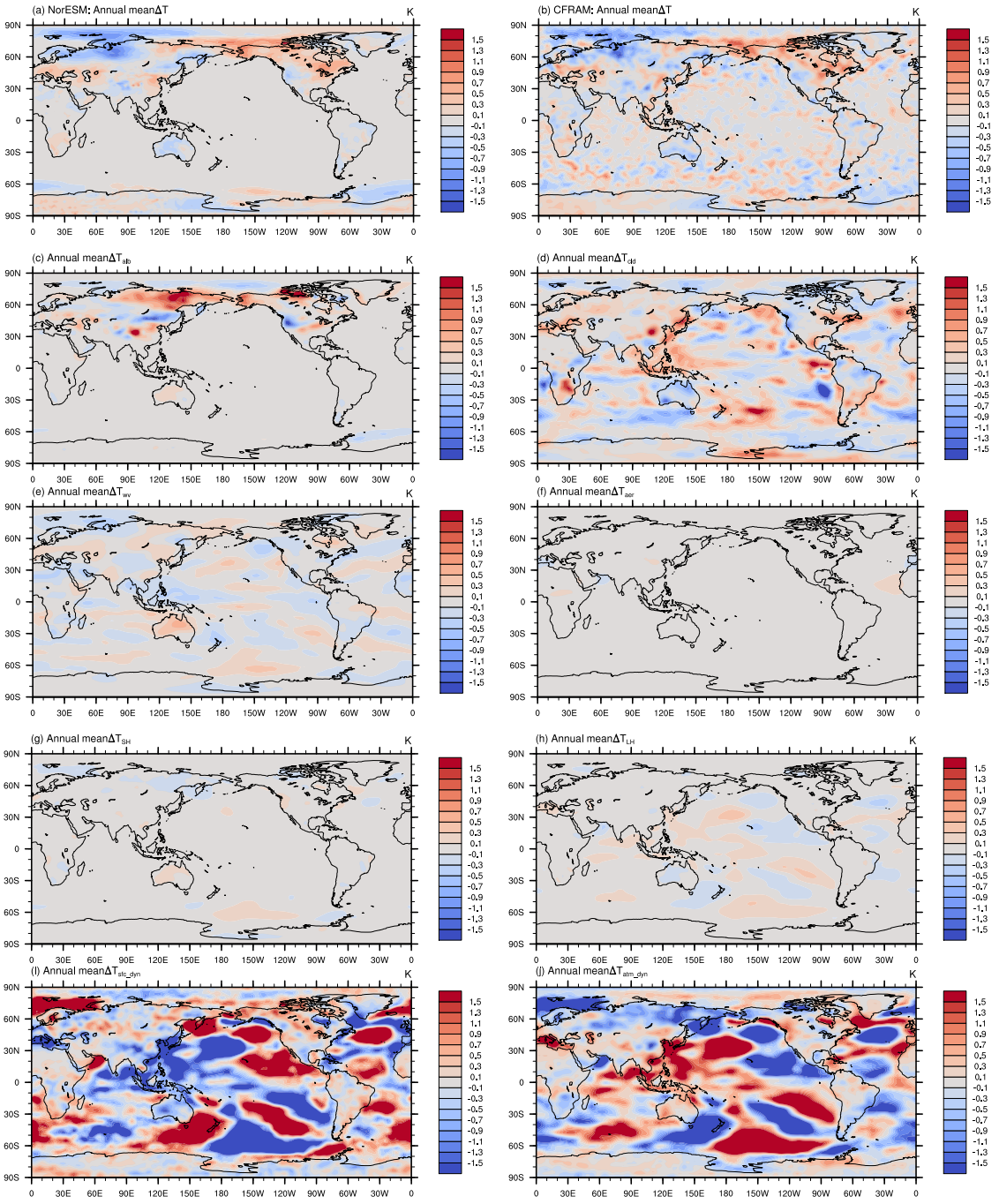

Figure 4.17: **a** Annual mean surface temperature difference from NorESM output, **b** Annual mean surface temperature difference derived from CFRAM, **c-j:** Annual mean partial surface temperature difference derived from CFRAM. **c** albedo, **d** cloud, **e** water vapor, **f** aerosol, **g** sensible heat, **h** latent heat, **i** surface dynamics, **j** atmosphere dynamics.

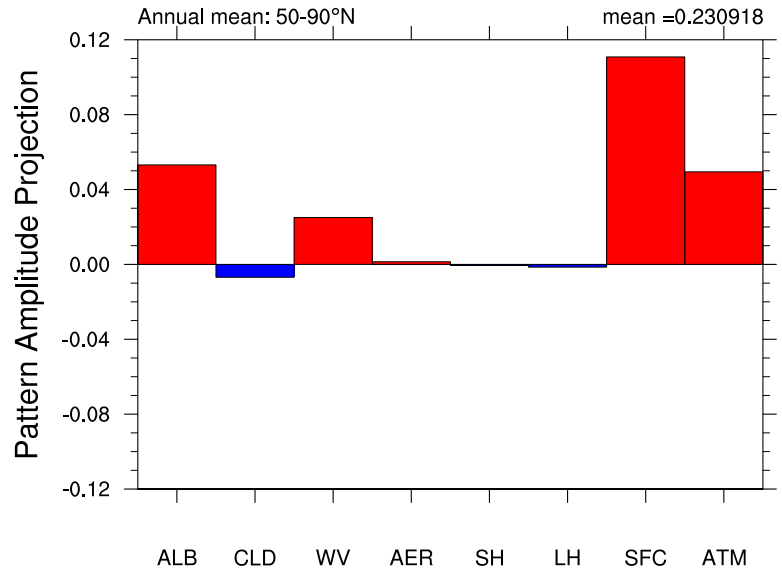

Figure 4.18: Pattern amplitude projection (PAP) coefficient of annually regional mean partial surface temperature differences of individual process: albedo, cloud, water vapor, aerosol, sensible heat, latent heat, surface dynamics and atmospheric dynamics.

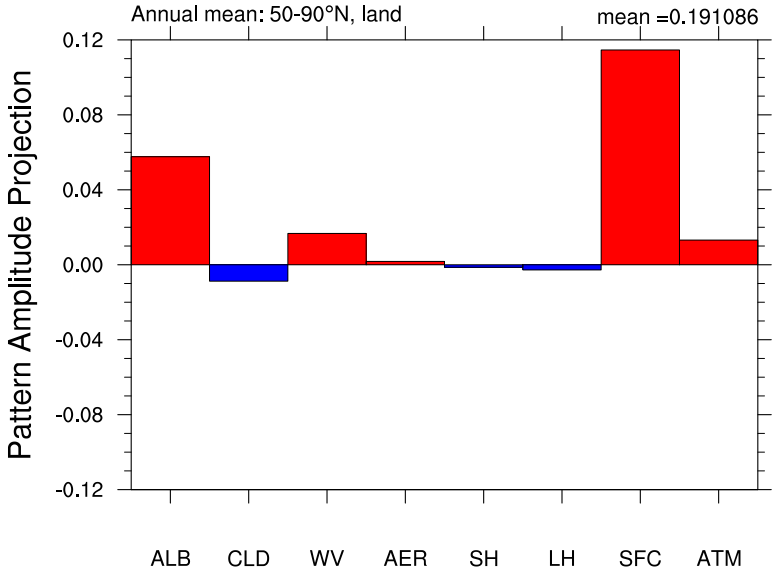

Figure 4.19: Pattern amplitude projection (PAP) coefficient of annually regional (only land) mean partial surface temperature differences of individual process: albedo, cloud, water vapor, aerosol, sensible heat, latent heat, surface dynamics and atmospheric dynamics.

4.3.2 Seasonal response

To explore the seasonal responses and contributions of individual feedback process with growing season lengthen, three seasonal surface temperature decompositions are analyzed. One case in April-May-June (AMJ) and one in August-September-October (ASO) which have the greatest increment of LAI, according to Fig. 3.2, and another one in June-July-August (JJA), in which season the peak of LAI reaches.

Fig. 4.20(a)-(b) show the April-May-June mean surface temperature differences, (a) is calculate from NorESM and (b) is derived from CFRAM. Fig. 4.20(c)-(j) show the partial surface temperature differences in April-May-June. Surface temperature shows large warming in Arctic ocean and mid-high latitude of Eurasia at the start of vegetation growing season and cooling in middle North America in AMJ. The albedo decreasing combine with the solar insolation increasing in spring-summer season, induces a significant albedo warming effect in NH high-latitude in AMJ (Fig. 4.20(c), Fig. 4.23(b)). Water vapor also exerts moderate warming in Arctic ocean and NH mid-high latitude, but cooling in North America (Fig. 4.20(e)). Cloud feedback produces warming in almost mid-high latitude, except middle North America (Fig. 4.20(d)). Aerosol and latent heat show relatively weaker impact on surface temperature in AMJ. Sensible heat cools in east Asia and north of North America (Fig. 4.20(g)). The surface dynamics exert strong cooling in east Asia and west North America (Fig. 4.20(i)). The atmospheric dynamics also cools in east Asia and north Atlantic Ocean (Fig. 4.20(i)&(j)).
Similarly, Fig. 4.21(a)-(b) show the June-July-August mean surface temperature differences, (a) is calculate from NorESM and (b) is derived from CFRAM. Fig. 4.21(c)-(j) show the partial surface temperature differences in June-July-August. The amplitude of surface temperature difference is relatively weaker in JJA than AMJ, even through LAI reaches peak in this period, but with little increment which lead to a weaker perturbation to climate system. Cloud shows relatively strong cooling effect over the land of mid-high latitude, a possible explanation to this result is that the solar insolation is the major incoming energy in Arctic and sub-Arctic in summer (JJA), but increasing clouds reduce the solar energy reach to surface. Cloud also exerts warming in NH mid-low latitude (Fig. 4.21(d)). Albedo effect in JJA is not as strong as AMJ, since the albedo differences is weaker than the starting period of growing season (Fig. 4.21(c)). Sensible heat shows relatively weak cooling in east Asia and north coast of North America (Fig. 4.21(g)). Surface dynamics and Atmospheric dynamics perform opposite pattern in NH high-latitude land. Surface dynamics shows strong warming in Arctic ocean, which counteract the cooling induced by albedo change (Fig. 4.21(i)&(j)).
Fig. 4.22(a)-(b) show the August-September-October mean surface temperature differences, (a) is calculate from NorESM and (b) is derived from CFRAM. Fig. 4.22(c)-(j) show the partial surface temperature differences in August-September-October. Surface temperature increases in middle latitude and decreases in Arctic. Partial temperature difference due to albedo effect moderately increase in east Asia and north part of North America (Fig. 4.22(c)). Cloud contributes significant warming in mid-low latitude and high latitude, but slightly cools the northern Arctic ocean (Fig. 4.22(d)). Water vapor warms in mid-high latitude but cools the Arctic ocean and low latitude (Fig. 4.22(e)). Aerosol, sensible heat and latent heat have less impact in autumn season, in the ASO. Surface dynamics exerts cooling effect in north Asia and warming in mid-low latitude (Fig. 4.22(i)), while atmospheric dynamics process cools in Arctic ocean and moderately warms over the continent of NH (Fig. 4.22(j)).

These seasonal analysis suggest that surface temperature is more sensitive to the start period of vegetation growing period lengthen than the later period, in other word, leaf area increasing in spring-summer will induces remarkable warming effects than leaf area increasing in autumn (Fig. 4.23(b)-(d)). Albedo feedback is the main radiative process contributing to surface temperature change in spring and summer, but the albedo effect rapidly weaken in autumn. Cloud consistently warms east Asia, which associates with more moisture in this area. While cloud cools the middle latitude of North America, also cloud cool most of Arctic region, because the expansion of leaf area induces cloud fraction increasing in Arctic, which reduce the amount of solar energy reaching surface. Water vapor shows similar effect of cloud with smaller amplitude of surface temperature contribution over land. Sensible heat exerts consistently and relatively weak cooling effect in middle latitude. In this study, with the lengthening of vegetation growing season, I expected to have acceptable aerosol effect, but the result shows little contribution of aerosol feedback. Latent heat process mainly impacts on ocean, and shows little impact over land.

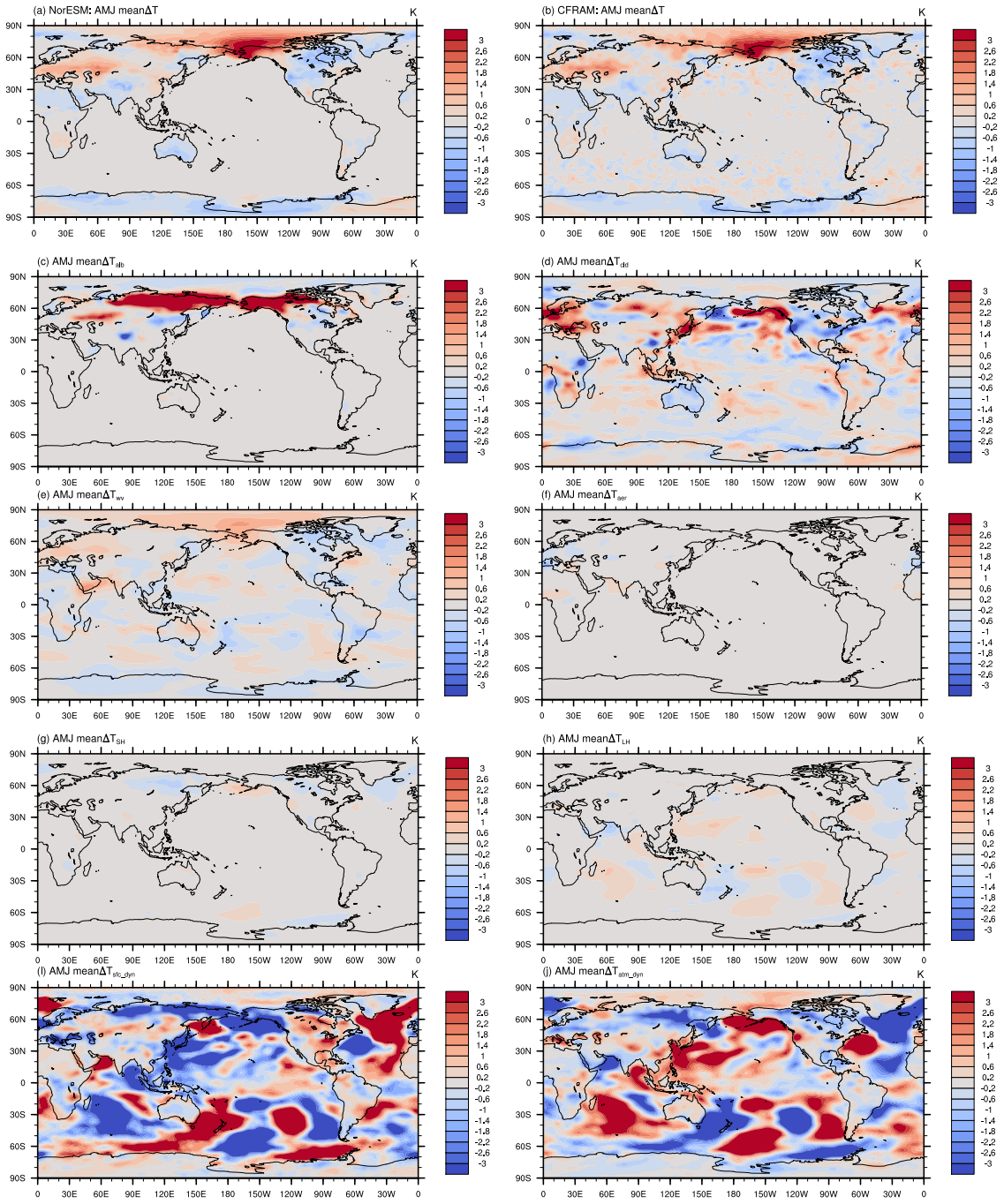

Figure 4.20: a April-May-June mean surface temperature difference from NorESM output, **b** April-May-June mean surface temperature difference derived from CFRAM, **c-j:** April-May-June mean partial surface temperature difference derived from CFRAM. **c** albedo, **d** cloud, **e** water vapor, **f** aerosol, **g** sensible heat, **h** latent heat, **i** surface dynamics, **j** atmosphere dynamics.

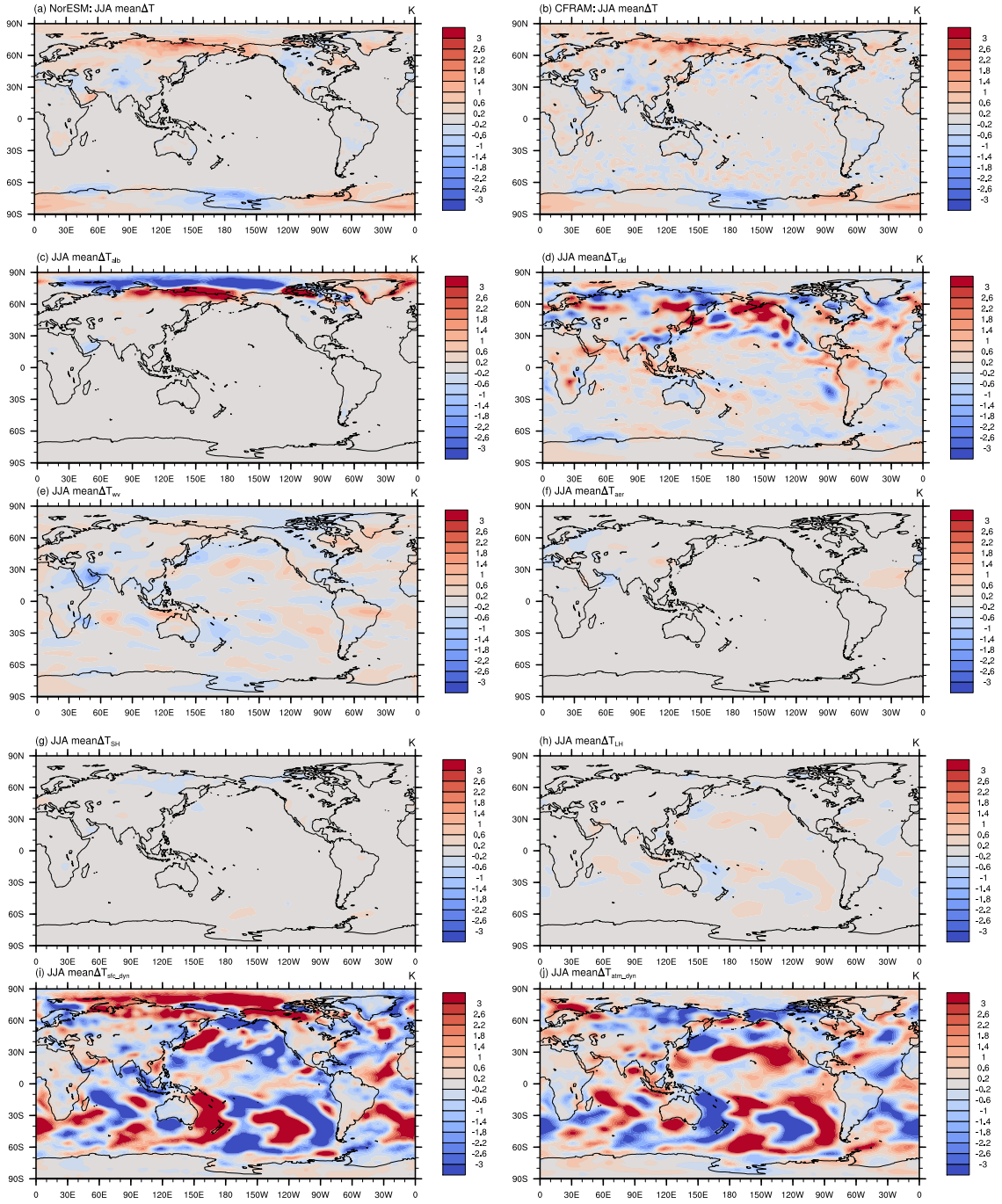

Figure 4.21: **a** June-July-August mean surface temperature difference from NorESM output, **b** June-July-August mean surface temperature difference derived from CFRAM, **c-j:** June-July-August mean partial surface temperature difference derived from CFRAM. **c** albedo, **d** cloud, **e** water vapor, **f** aerosol, **g** sensible heat, **h** latent heat, **i** surface dynamics, **j** atmosphere dynamics.

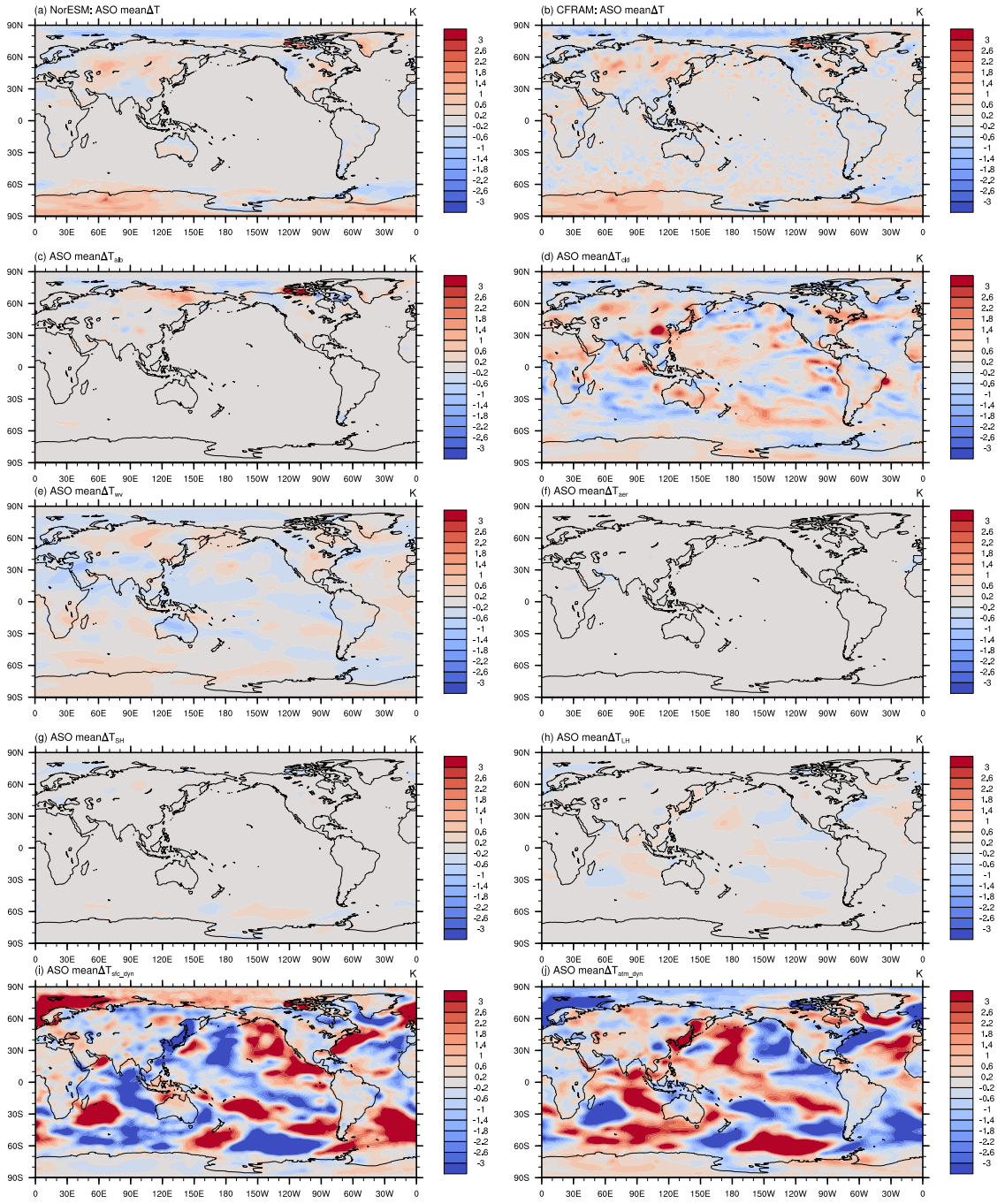

Figure 4.22: a August-September-October mean surface temperature difference from NorESM output, **b** August-September-October mean surface temperature difference derived from CFRAM, **c-j:** August-September-October mean partial surface temperature difference derived from CFRAM. **c** albedo, **d** cloud, **e** water vapor, **f** aerosol, **g** sensible heat, **h** latent heat, **i** surface dynamics, **j** atmosphere dynamics.

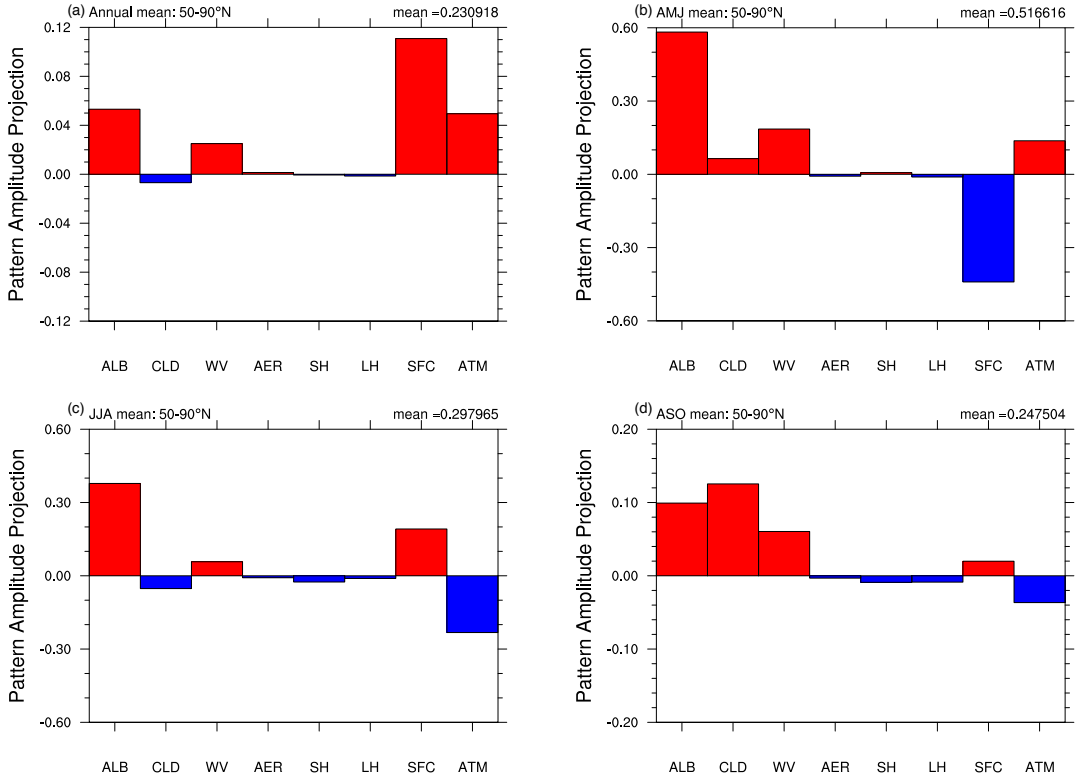

Figure 4.23: Pattern amplitude projection (PAP) coefficient of regional mean partial surface temperature differences of individual process: albedo, cloud, water vapor, aerosol, sensible heat, latent heat, surface dynamics and atmospheric dynamics.**a** Annually, **b** April-May-June, **c** June-July-August, **d** August-September-October.

Chapter 5

Summary and Conclusion

With the expansion of vegetation growing season, climate shows significant signals associated with individual climate feedback. To study the contribution of each feedback process, the CFRAM analysis method is applied. CFRAM is a technique which has been used to decompose the temperature contributions of individual feedback process. When calculating off-line radiative transfer model experiments, I found that use of hourly data is necessary for obtaining the acceptable representation of radiative fluxes, especially for the experiment with perturbations of cloud and albedo, which have relatively large daily variation. In the radiative transfer model, the McICA is used to reduce the errors induced by unresolved cloud fluctuations, but it induces an inevitable noise. The increase of sample numbers in McICA gives a significant reduction of noise. The result with 400 sample numbers gives a moderate improvement compared with 200 sample numbers. That suggest the increase of sample number could efficiently decrease the noise but it also has limitation. I also verified the different input variables of clouds in the off-line radiative transfer model; the cloud water path and cloud optical depth. The result suggest that the water vapor path shows better representation than cloud optical depth. For CFRAM analysis method, it is important to understand the dynamic part. The radiative terms in CFRAM equations could directly be derived with radiative transfer model, but the dynamic terms, which contain the energy transport due to convection and large-scale advection in atmosphere and the horizontal energy exchange in the surface layer is derived from the energy balance equation by calculating the difference between total radiative energy change and latent heat and sensible heat changes.

Growing season expansion in Arctic leads to warming in the region with decreasing albedo associated with the expansion of growing season in 50-80°N. The surface temperature in Arctic shows largest increase at the start of growing season and relatively weaker increase at the end of growing season. The change of albedo gives a significant decrease in Arctic at the start of growing season and relatively small decrease at the end of growing season. These seasonal changes in surface temperature and albedo correspond to the LAI modification which represents the expansion of growing season. The results suggest that albedo is more sensitive to vegetation changes during the start of growing season (spring-summer) than the end of growing season (summer-autumn). Over land, sensible heat has a significant increase in the LAI modified region while latent heat has a moderate increase. The change of humidity near the surface increases over most areas between 50-80°N, which corresponds to the change of LAI, The decrease in mid-low latitude may be caused by the water vapor transport to high-latitude by circulation. Humidity also has a decrease in low-mid latitude and the north ocean of Eurasia and the north continent of Europe. The cloud cover decreases in north pole but increases in 50-80°N, that suggest the increase of LAI will increase the cloud amount locally. The reduction of cloud near the north pole is associated with the decrease of water vapor in this area. The surface temperature, albedo, sensible heat, humidity and cloud have a pronounced positive

response to the lengthening of growing season in LAI modified area. The results also suggest that the changes of Arctic vegetation may have impact in lower latitude through the circulation.

In the decomposition of annual mean surface temperature of individual feedbacks, the temperature contribution of albedo shows the largest amplitude over land in these radiative processes. The albedo-driven temperature significantly rises in the LAI increased area in the Arctic. The cloud-driven temperature shows moderate warming in most land area of 50-80°N and weak cooling in northern of 80°N. The water vapor effect warms most land areas of 50-80°N, except the northwest of Eurasia, which is associated with the lack of water vapor. The aerosol and latent heat have little impact on surface temperature over land. Sensible heat gives a weak negative contribution in east Asia and the ocean at the north side of Europe. The amplitude of the temperature contribution of surface dynamic and atmosphere dynamic processes is comparable to the contribution of albedo. Except the dynamic processes, the albedo effect shows the primary contribution to surface temperature change. Temperature contribution of water vapor is half of the albedo effect, while the cloud effect presents a weak negative contribution to surface temperature in Arctic. Sensible heat and latent heat have little impact on surface temperature in Arctic continent. Since the lengthening of growing season increased the LAI, I expected the response of latent heat would be pronounced with the increased evapotranspiration, but the result seems to give less response to growing season expansion. The decomposition of seasonal mean temperature reveals that these feedback are most pronounced at the start period of growing season (spring-summer). Clouds have a positive contribution in the starting period over land. In the period with the peak of LAI, cloud effect has a significant negative contribution to temperature changes in the LAI modified area. A explanation for this is that during the summer season, when the zenith angle is smallest, with highest incoming solar insolation of the year, but the increase of LAI due to growing season expansion induces the increase of evapotranspiration and consequently increases the cloud cover. The increased cloud cover tends to reflect more solar insolation to space, then the absorption of solar energy at surface is decreasing. The response at the end of growing season is weaker than starting period.

Chapter 6

Future Work

The application of fully coupled model with active ocean mode

In this work, I did the experiments with prescribed ocean and sea-ice since time was limited. That made me miss the signals of sea-ice, which are important in Arctic climate research. In Bhatt et al., 2010's work, they present the result that the change of maximum Normalized Difference Vegetation Index (NDVI) in northern Alaska and the Beaufort Sea region was highly linked to the strong retreat of sea ice, that the vegetation change in high-latitude is likely associated with rapid sea ice declines. Then, it is interesting to investigate how sea-ice respond to the vegetation change.

Application of CFRAM to other climate research

The climate feedback response analysis method (CFRAM) applied in this work is an new and useful analysis tool for studying different feedback process in climate system, and it also can also be used in other future studies.

The impact of different vegetation changes

The growing season of vegetation is manually expanded for all selected Arctic vegetation type. Loranty, Goetz, and Beck, 2011 study the tundra vegetation change effects on albedo. The result shows that the changes in net radiation associated with differences in vegetation type at weekly time scales may be up to 50 Wm^{-2}, this suggests that different vegetation type may have different impacts. Further study on impact of different vegetation types could give better understanding of vegetation trigged energy budget changes.

Bibliography

Andreu-Hayles, Laia et al. (2011). "Varying boreal forest response to Arctic environmental change at the Firth River, Alaska". In: *Environmental Research Letters* 6.4, p. 045503.

Barker, HW et al. (2008). "The Monte Carlo independent column approximation: an assessment using several global atmospheric models". In: *Quarterly Journal of the Royal Meteorological Society* 134.635, pp. 1463–1478.

Beck, Pieter SA and Scott J Goetz (2011). "Satellite observations of high northern latitude vegetation productivity changes between 1982 and 2008: ecological variability and regional differences". In: *Environmental Research Letters* 6.4, p. 045501.

Bentsen, Mats et al. (2013). "The Norwegian earth system model, NorESM1-M—Part 1: description and basic evaluation of the physical climate". In: *Geosci. Model Dev* 6.3, pp. 687–720.

Beringer, Jason et al. (2005). "Surface energy exchanges along a tundra-forest transition and feedbacks to climate". In: *Agricultural and Forest Meteorology* 131.3, pp. 143–161.

Bhatt, Uma S et al. (2010). "Circumpolar Arctic tundra vegetation change is linked to sea ice decline". In: *Earth Interactions* 14.8, pp. 1–20.

Bonfils, CJW et al. (2012). "On the influence of shrub height and expansion on northern high latitude climate". In: *Environmental Research Letters* 7.1, p. 015503.

Cai, Ming and Jianhua Lu (2009). "A new framework for isolating individual feedback processes in coupled general circulation climate models. Part II: Method demonstrations and comparisons". In: *Climate dynamics* 32.6, pp. 887–900.

Chapin III, F Stuart et al. (2000). "Summer differences among arctic ecosystems in regional climate forcing". In: *Journal of Climate* 13.12, pp. 2002–2010.

Chen, Yonghua et al. (2011). "Projected regime shift in Arctic cloud and water vapor feedbacks". In: *Environmental Research Letters* 6.4, p. 044007.

Clough, SA et al. (2005). "Atmospheric radiative transfer modeling: a summary of the AER codes". In: *Journal of Quantitative Spectroscopy and Radiative Transfer* 91.2, pp. 233–244.

Deng, Yi, Tae-Won Park, and Ming Cai (2012). "Process-based decomposition of the global surface temperature response to El Niño in boreal winter". In: *Journal of the Atmospheric Sciences* 69.5, pp. 1706–1712.

Earth's Radiation Budget Facts (2011). URL: https://science-edu.larc.nasa.gov/EDDOCS/radiation_facts.html.

Epstein, Howard E, Isla Myers-Smith, and Donald A Walker (2013). "Recent dynamics of arctic and sub-arctic vegetation". In: *Environmental Research Letters* 8.1, p. 015040.

Fehsenfeld, Fred et al. (1992). "Emissions of volatile organic compounds from vegetation and the implications for atmospheric chemistry". In: *Global Biogeochemical Cycles* 6.4, pp. 389–430.

Fraser, RH et al. (2011). "Detecting long-term changes to vegetation in northern Canada using the Landsat satellite image archive". In: *Environmental Research Letters* 6.4, p. 045502.

Hansen, J et al. (1983). "Efficient three-dimensional global models for climate studies: Models I and II". In: *Monthly Weather Review* 111.4, pp. 609–662.

Hu, Xiaoming et al. (2017). "Process-based Decomposition of the Decadal Climate Difference between 2002-13 and 1984-95". In: *Journal of Climate* 2017.

Jeong, Jee-Hoon et al. (2012). "Greening in the circumpolar high-latitude may amplify warming in the growing season". In: *Climate dynamics* 38.7-8, pp. 1421–1431.

Jeong, Su-Jong et al. (2011). "Impact of vegetation feedback on the temperature and its diurnal range over the Northern Hemisphere during summer in a 2× CO2 climate". In: *Climate dynamics* 37.3-4, pp. 821–833.

Kaplan, Jed O and Mark New (2006). "Arctic climate change with a 2 C global warming: Timing, climate patterns and vegetation change". In: *Climatic change* 79.3-4, pp. 213–241.

Kay, Jennifer E et al. (2016). "Recent advances in Arctic cloud and climate research". In: *Current Climate Change Reports* 2.4, pp. 159–169.

Kirkevåg, A et al. (2013). "Aerosol–climate interactions in the Norwegian Earth System Model–NorESM1-M". In: *Geoscientific Model Development* 6.1, pp. 207–244.

Laguë, Marysa M and Abigail LS Swann (2016). "Progressive midlatitude afforestation: Impacts on clouds, global energy transport, and precipitation". In: *Journal of Climate* 29.15, pp. 5561–5573.

Lin, DH et al. (2012). "High spatial resolution decade-time scale land cover change at multiple locations in the Beringian Arctic (1948–2000s)". In: *Environmental Research Letters* 7.2, p. 025502.

Liu, Zhengyu et al. (2006). "Assessing global vegetation–climate feedbacks from observations". In: *Journal of Climate* 19.5, pp. 787–814.

Loranty, Michael M, Scott J Goetz, and Pieter SA Beck (2011). "Tundra vegetation effects on pan-Arctic albedo". In: *Environmental Research Letters* 6.2, p. 024014.

Loranty, Michael M et al. (2014). "Vegetation controls on northern high latitude snow-albedo feedback: observations and CMIP5 model simulations". In: *Global change biology* 20.2, pp. 594–606.

Lu, Jianhua and Ming Cai (2009). "A new framework for isolating individual feedback processes in coupled general circulation climate models. Part I: Formulation". In: *Climate dynamics* 32.6, pp. 873–885.

Miller, Paul A and Benjamin Smith (2012). "Modelling tundra vegetation response to recent arctic warming". In: *Ambio* 41.3, pp. 281–291.

Myers-Smith, Isla H et al. (2015). "Climate sensitivity of shrub growth across the tundra biome". In: *Nature Climate Change* 5.9, p. 887.

Ohse, B, F Jansen, and M Wilmking (2012). "Do limiting factors at Alaskan treelines shift with climatic regimes?" In: *Environmental Research Letters* 7.1, p. 015505.

Pachauri, R. K. et al. (2014). *Climate Change 2014: Synthesis Report. Contribution of Working Groups I, II and III to the Fifth Assessment Report of the Intergovernmental Panel on Climate Change*. Ed. by R.K. Pachauri and L. Meyer. Geneva, Switzerland: IPCC, p. 151.

Park, Tae-Won et al. (2014). "A dissection of the surface temperature biases in the Community Earth System Model". In: *Climate dynamics* 43.7-8, pp. 2043–2059.

Pearson, Richard G et al. (2013). "Shifts in Arctic vegetation and associated feedbacks under climate change". In: *Nature climate change* 3.7, p. 673.

Pielke, Roger A et al. (1998). "Interactions between the atmosphere and terrestrial ecosystems: influence on weather and climate". In: *Global change biology* 4.5, pp. 461–475.

Räisänen, P, Howard W Barker, and JNS Cole (2005). "The Monte Carlo Independent Column Approximation's conditional random noise: Impact on simulated climate". In: *Journal of climate* 18.22, pp. 4715–4730.

Richardson, Andrew D et al. (2013). "Climate change, phenology, and phenological control of vegetation feedbacks to the climate system". In: *Agricultural and Forest Meteorology* 169, pp. 156–173.

Seddon, AW et al. (2016). "Sensitivity of global terrestrial ecosystems to climate variability". In: *Nature* 531.7593, pp. 229–232.

Serreze, Mark C and Roger G Barry (2011). "Processes and impacts of Arctic amplification: A research synthesis". In: *Global and Planetary Change* 77.1, pp. 85–96.

Serreze, MC et al. (2009). "The emergence of surface-based Arctic amplification". In: *The Cryosphere* 3.1, p. 11.

Shupe, Matthew D and Janet M Intrieri (2004). "Cloud radiative forcing of the Arctic surface: The influence of cloud properties, surface albedo, and solar zenith angle". In: *Journal of Climate* 17.3, pp. 616–628.

Song, Xiaoliang, Guang J Zhang, and Ming Cai (2014). "Characterizing the climate feedback pattern in the NCAR CCSM3-SOM using hourly data". In: *Journal of Climate* 27.8, pp. 2912–2930.

Stephens, Graeme L and Tristan L'Ecuyer (2015). "The Earth's energy balance". In: *Atmospheric Research* 166, pp. 195–203.

Stephens, Graeme L et al. (2012). "An update on Earth's energy balance in light of the latest global observations". In: *Nature Geoscience* 5.10, p. 691.

Swann, Abigail L et al. (2010). "Changes in Arctic vegetation amplify high-latitude warming through the greenhouse effect". In: *Proceedings of the National Academy of Sciences* 107.4, pp. 1295–1300.

Sykes, Martin T (2009). "Climate change impacts: Vegetation". In: *eLS*.

Tremblay, Benoît, Esther Lévesque, and Stéphane Boudreau (2012). "Recent expansion of erect shrubs in the Low Arctic: evidence from Eastern Nunavik". In: *Environmental Research Letters* 7.3, p. 035501.

Trenberth, Kevin E et al. (2015). "Climate variability and relationships between top-of-atmosphere radiation and temperatures on Earth". In: *Journal of Geophysical Research: Atmospheres* 120.9, pp. 3642–3659.

Vavrus, Steve et al. (2009). "Simulations of 20th and 21st century Arctic cloud amount in the global climate models assessed in the IPCC AR4". In: *Climate Dynamics* 33.7-8, p. 1099.

Zhang, H, X Jing, and J Li (2014). "Application and evaluation of a new radiation code under McICA scheme in BCC_AGCM2. 0.1". In: *Geoscientific Model Development* 7.3, p. 737.